• U C •
FCTUC FACULDADE DE CIÊNCIAS
E TECNOLOGIA
UNIVERSIDADE DE COIMBRA

Inês Isabel Geraldes Vaz

Computational modelling of brain states

Dissertation presented to the University of Coimbra in fulfilment of the requirements to obtain a Master's degree in Biomedical Engineering

Supervisors:

Dr. Maria Ribeiro (Institute for Biomedical Imaging and Life Sciences, Faculty of Medicine, University of Coimbra)

Dr. Joana Cabral (Department of Psychiatry, University of Oxford)

Coimbra, 2016

This work was developed in collaboration with:

Institute for Biomedical Imaging and Life Sciences, Faculty of Medicine, University of Coimbra

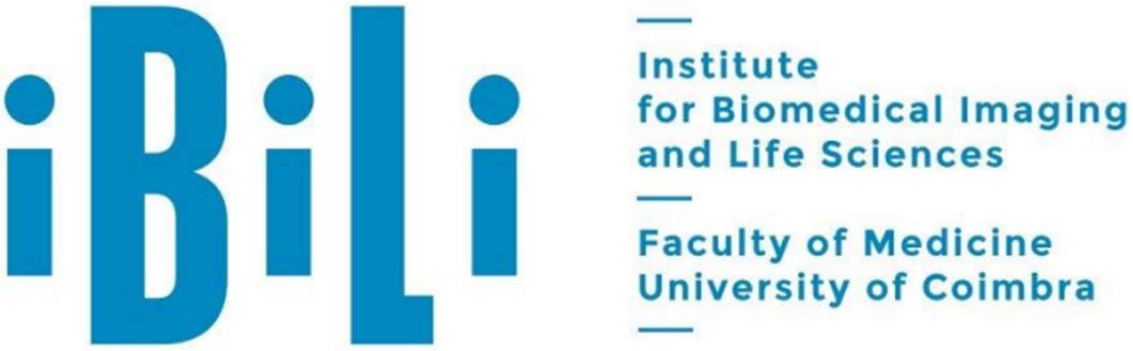

the thesis and no information derived from it may be published without proper acknowledgement.

Acknowledgements

Quero em primeiro lugar agradecer às minhas orientadoras Maria Ribeiro e Joana Cabral, que idealizaram um projeto que me permitiu aplicar conhecimentos adquiridos ao longo do curso numa área que sempre me fascinou: a neurociência. Agradeço em particular à Dra. Maria pelo apoio incondicional, pela paciência e inúmeras sugestões que tornaram este trabalho possível. Agradeço também à Dra. Joana pela sua disponibilidade em ajudar sempre que possível, apesar da distância; e claro por ter desenvolvido o modelo computacional usado neste projeto, que vários contributos já deu e continuará a dar neste longo caminho que é a revelação dos segredos do cérebro.

Não posso também deixar de agradecer aos professores e colegas que contribuiram para a aquisição das competências que me permitiram realizar este projeto. Agradeço especialmente à Tânia, não só pela amizade sincera, mas também por ser uma fonte de inspiração, um verdadeiro exemplo de empenho e dedicação.

Por fim, agradeço à minha família e amigos o apoio que foi e sempre será fundamental para o sucesso dos meus empreendimentos. Agradeço em particular aos meus pais, à minha irmã e ao Rodrigo.

Abstract

Activities such as sleeping, resting, meditating and performing a task demand different types and levels of information processing in the brain. Accordingly, this complex organ seems to adopt different modes of processing that endow it with distinguishable global characteristics. Numerous functional imaging studies have been characterizing such states, including the associated neural networks, functional connectivity patterns and graph theory properties. However, the mechanisms that trigger each of these states, altering the spontaneous dynamics of the brain, remain a fundamental open question in neuroscience.

In this thesis, we investigate how changes in connectivity strengths may contribute to cause the observable global dynamics change during the performance of a task. To do that, we use a large-scale model of resting-state activity where the coupling strength between regions can be manipulated. We attempted to constrain the simulated activity to behave as a task-state by altering two different sets of connections by a range of coupling values. These connections were chosen according to empirical findings that show alterations during task performance.

Notably, for specific values of coupling, simulations of both changes in connectivity strengths were able to reproduce important global properties of the task state, specifically a decrease in functional connectivity variability, an overall increase in the nodes strength and significant alterations in functional integration and segregation.

Our results not only suggest two possible mechanisms that may explain alterations of global dynamics in the task state, but also highlight the ability of computational modelling to suggest relevant hypotheses relative to large-scale brain functioning.

Resumo

Actividades como dormir, descansar, meditar ou realizar uma tarefa exigem diferentes tipos e níveis de processamento de informação no cérebro. Em consequência, este órgão complexo parece adoptar diferentes modos de processamento que o dotam de características globais distintas. Numerosos estudos de imagiologia funcional têm vindo a caracterizar esses estados, incluindo as redes neuronais que lhes estão associadas, padrões de conectividade funcional e propriedades da teoria de grafos. Porém, os mecanismos que causam cada um destes estados, alterando a dinâmica espontânea do cérebro, permanecem uma questão fundamental em aberto na neurociência.

Nesta tese, investigamos como alterações nas forças de ligação poderão contribuir para causar a mudança na dinâmica global do cérebro observável durante a realização de tarefas. Para tal, foi usado um modelo da actividade do cérebro em grande escala durante o repouso, em que é possível manipular a força das ligações entre regiões cerebrais. Tentámos compelir a actividade simulada a comportar-se como a encontrada na realização de tarefas, através da alteração de dois conjuntos diferentes de ligações, numa certa gama de valores de acoplamento. Essas ligações foram escolhidas com base em resultados empíricos que mostram alterações durante a execução de tarefas.

Notavelmente, para valores específicos de acoplamento, as simulações de ambas as alterações nas forças de ligação foram capazes de reproduzir propriedades globais importantes, como uma diminuição na variabilidade da conectividade funcional, um aumento global da força dos nodos e alterações significativas na integração e na segregação funcional.

Os nossos resultados não só sugerem dois mecanismos que poderão explicar as alterações na dinâmica global do cérebro observada no estado de tarefa, mas também realçam a capacidade da modelação computacional para sugerir hipóteses relevantes em relação ao funcionamento do cérebro em grande escala.

Contents

List of abbreviations

AAL	Automated Anatomical Labelling
ACC	Anterior Cingulate Cortex
BOLD	Blood-Oxygen-Level Dependent
BA	Brodmann Area
DAN	Dorsal Attention Network
DMN	Default Mode Network
EEG	Electroencephalography
FC	Functional Connectivity
FPCN	Frontoparietal Control Network
fMRI	Functional Magnetic Resonance Imaging
ICA	Independent Component Analysis
MEG	Magnetoencephalography
MRI	Magnetic Resonance Imaging
PCC	Posterior Cingulate Cortex
SAL	Salience Network
SC	Structural Connectivity
TPN	Task-Positive Network
VAN	Ventral Attention Network

1 | INTRODUCTION

1.1 | Motivation and goals

Understanding how neural processes give rise to cognition is a central goal of neuroscience. The mechanisms behind this phenomenon have been progressively revealed using different approaches, with a traditional bias towards empirical methods. However, computational models of the brain can provide an important tool for understanding its complexity and numerous studies using them have already given substantial contributions to the field. One important application of these models is the investigation of the effects of anatomical alterations, such as lesions, in the brain dynamics. Interpreting such effects in experimental data is difficult because of the complexity of the underlying neural architecture.

The main goal of this thesis was to investigate mechanisms that might explain the observed alterations of global dynamics in the task state. We investigated using a computational model of the human brain if the switch between different attentional states, resting-state and task performance, can be achieved by changes in the connectivity strength between specific brain regions. We were inspired by empirical studies that suggested that changes in connectivity strength between and within attentional networks were associated with attentional control. We compared the results between our simulation studies with empirical data to define the resting-state and the task state and further analysed the properties of these states using graph theory measures.

1.2 | Theoretical background

1.2.1 | Structural and functional connectivity of the brain

The brain has always fascinated and intrigued us, but due to its intricate structure and wide variety of functions, it remains the least understood human organ. However, the development of sophisticated technological tools allows scientists to progressively disentangle the complex mechanisms of brain functioning. Studies of the architecture of the brain, either using histological or imaging techniques, reveal a complex network organization at multiple scales (Sporns et al., 2000). The structural connections, mainly constituted of axonal fibres, support the communication between specialized brain areas, enabling integration of segregated information and processing.

This chapter summarizes the current knowledge of the connectivity of the brain, distinguishing between structural and functional connectivity. Although a functional bond usually exists between regions that share an anatomical link (Hagmann et al., 2008; Koch et al., 2002; Honey et al., 2009), the opposite is not necessarily true, since functional connectivity has been observed in the absence of a direct anatomical connection (Koch et al., 2002).

1.2.1.1 | Anatomical connectivity

The ultimate aim of connectomics is to obtain the map of all neural connections of the human brain or connectome (Hagmann, 2005; Sporns et al., 2005), one of the holy grails of neuroscience. Given that the human brain probably encompasses several billions of neurons, this achievement will demand decades of research, as well as contributions from diverse techniques and approaches.

C. elegans, a one-millimeter long worm with 300 neurons and 7000 connections, is the only species which complete nervous system has been mapped so far. This deduction was made by White et al. (1986) through reconstruction of electron micrographs, mostly done by hand, a technique that allows mapping at the cellular level but is extremely time-consuming.

A more efficient mapping can be achieved using Diffusion Tensor Imaging (DTI). DTI is a magnetic resonance imaging (MRI) modality that detects restricted diffusion of water in

tissues (anisotropic diffusion) and estimates its direction and strength, thus inferring the localization of white matter pathways. Tractography algorithms then use DTI data to reconstruct neural tracts as three-dimensional curves.

The first human brain mappings using DTI were obtained in 2007 (Hagmann et al., 2007; Iturria-Medina et al., 2007). While Hagmann's connectomes divided the brain into 500 to 4000 regions and were derived from the brains of two healthy subjects, Iturria-Medina's had lower resolution, with 71 areas, and were based on the brains of five healthy subjects.

The connectome's resolution depends on the parcellation scheme used, which determines the number of regions into which the brain is divided. Several parcellation schemes have been applied in the history of neuroscience, ranging from four to several thousand regions of interest. One of the first and most widely known is the Brodmann's division (1909), which 52 areas were defined using staining methods, and therefore exclusively based on the cytoarchitectural organization of neurons. Due to the high number of existing parcellation schemes, Tzourio-Mazoyer et al. (2002) proposed a standardized anatomical division, the Automated Anatomical Labelling (AAL) scheme, which has become one of the most used parcellation schemes. The AAL brain is divided into eight classes – grey matter, white matter, glial matter, cerebrospinal fluid, fat, muscle/skin, skin and skull –, after which the grey matter is further divided into 90 regions.

1.2.1.2 | Functional connectivity

Two regions that exhibit a high temporal correlation are said to be functionally connected. Therefore, functional connectivity (FC) is generally derived from brain activity time series observations and describes patterns of statistical dependence among brain regions (Smith 2012). It must be noted however that while the presence of a statistical relationship between two regions often predicts functional coupling, the existence of such coupling does not imply a causal relationship (Smith et al., 2011).

Time series data can be obtained using a variety of techniques, including electroencephalography (EEG), magnetoencephalography (MEG) and functional magnetic resonance imaging (fMRI). EEG (electrophysiological activity recorded outside the scalp) can be recorded by placing electrodes in the scalp and has a high temporal resolution (around 1

ms), in addition to being relatively cheap, portable and easy to implement. However, physical limitations implicate a low spatial resolution (several centimetres) and almost impossible detection of electric activity from deep sources. MEG is a technique that measures magnetic fields produced by electrical currents in the scalp. Although MEG can only detect the tangential components of cortical activity, its spatial resolution is far superior to EEG's (millimetre precision), while its temporal precision is very similar (1 ms). Functional MRI, probably the most popular functional neuroimaging technique, uses the blood-oxygen-level dependent (BOLD) contrast (Ogawa et al., 1990) to detect blood oxygenation differences, an indirect measure of neuronal activity, thus generating the so-called BOLD signals. Functional MRI has a high spatial resolution (usually 1-6 mm) and a low temporal precision (1 or 2 seconds), but high enough to distinguish between trials, since most fMRI experiments investigate brain processes that last several seconds. In here, we focus on signals acquired with fMRI, as this is the signal we will model in this thesis.

After fMRI acquisition, multiple approaches may be implemented to extract patterns of co-activation from the signals of each region. The most widely used method is the estimation of the linear (Pearson) correlation coefficient between BOLD signals; when two regions continually activate (BOLD increase) and deactivate (BOLD decrease) at the same time, their correlation is high (≈ 1), indicating the presence of a functional connection. Correlation data can then be used to derive functional networks by either studying seed-based correlations or the correlation matrix. In the first mentioned approach, the main activations sites of a certain network (seeds) must be defined; correlation maps of each seed are computed and overlapped to obtain maps of seed coactivations; the brain regions that correlate with each seed are identified as part of the network. In the second approach, the correlation matrix is computed; each line of the matrix corresponds to a brain region and the entries in that line correspond to the correlation coefficient between the signal in that region and all remaining regions (columns). Graph theory – the mathematical study of networks – may then be used to study the topological properties of each node and determine the most coupled regions. The connectome is in that case represented as a graph: a set of nodes, each representing a brain region, linked by edges, which symbolize the connections between them.

Another useful approach to define functional networks is Independent Component Analysis (ICA). ICA assumes that the signal acquired from each region results from the superposition

of statistically independent signals originating from different sources. This computational method maps the brain areas that contribute to each independent component; from these results, it is possible to obtain the spatial map of each independent component, corresponding to each functional network. ICA is particularly useful because it does not require a predefinition of "seeds" locations, as correlation approaches do.

1.2.2 | Brain modes: task and rest

Depending on information processing demands, the brain seems to adopt different modes, as will become clear in this section. Using functional imaging, it is possible to distinguish between them, by analysing reliable patterns of co-activation and/or connectivity of multiple brain areas. Specifically, several differences have been observed between the resting-state and during performance of tasks with an external focus of attention. While the first mainly engages the default mode network (DMN), which has been associated to mind-wandering and internally-directed cognition, the second activates different networks dedicated to external attention. In this section, we describe the signatures of these two brain sets, including associated networks, functional connectivity patterns and global functional properties.

1.2.2.1 | Associated networks

1.2.2.1.1 | Default mode network

Functional neuroimaging studies focused primarily in observing brain activity during the performance of specific tasks or after external stimulation. The images acquired in a task state would be subtracted from images acquired in a control state, displaying localized activity differences. Increases of activity, or activations, should be expected in these subtractions, however several studies revealed a set of regions that recurrently exhibited deactivations during the task states.

Shulman et al. (1997) presented the first formal characterization of task-induced deactivations in a meta-analysis of 9 PET studies, involving 134 subjects. This analysis revealed a set of brain regions more active during passive task conditions than during goal-directed task conditions. Similar results were obtained by Binder et al. (1999) and Mazoyer

et al. (2001), using identical approaches, and continued to be observed in hundreds of studies, until today.

The term “default mode of brain function” was first used by Raichle, Gusnard and colleagues in 2001, to describe the baseline state of the human brain. In an influential series of three papers, they not only addressed the problem of defining a baseline but also considered possible functions for the resting state activity. Their reviews clearly indicated that this default mode network (DMN) should be explored as its own area of study and considered as an independent brain system, with distinct physiological and cognitive properties, much like the visual or the motor system.

The regions consistently identified in the DMN are the medial prefrontal cortex [Brodmann areas (BA) 9, 10, 32], the posterior cingulate/retrosplenial cortex (PCC/Rsp) (BA 29/30, 23/31), the inferior parietal cortex (BA 39, 40), the lateral temporal cortex (BA 21) and the hippocampal formation (including hippocampus proper, entorhinal and parahippocampal cortex) (Buckner et al., 2008). The hippocampal region has been less consistently observed than the others, which may be explained by either its role in the DMN, or variation in its measurement, due for instance to the high diurnal variations that hippocampal-parietal memory network exhibits (sleep seems to reset this relationship) (Shannon et al., 2013).

Several changes in the DMN pattern related to the engagement in a task have been reported, including a greater recruitment of ACC relative to PCC, when switching from a lower to higher working memory loads, as well as an absent coactivation with hippocampus, usually found during rest (Esposito et al., 2006). In another study, the functional connectivity of the inferior temporal gyrus (ITG) with other DMN regions was found enhanced in a semantic judgment task. Further, Uddin et al. (2009) noticed that activity in ventral medial prefrontal cortex negatively predicted activity in parietal visual spatial and temporal attention networks, whereas PCC activations negatively predicted activity in prefrontal-based motor control circuits, suggesting that these two major nodes of DMN may interact differentially with task-positive regions. These findings suggest high heterogeneity within this network and indicate that information processing in DMN regions may be task dependent.

DMN is hypothesized to mediate task-independent thoughts, or internal mentation, because its regions have been found activated when subjects engage in self-generated thoughts and deactivated during tasks that require an attentional focus in the external world. The more DMN activity is suppressed, the better people perform on tasks involving extrinsic stimulus processing: activity in the DMN increases during lapses in external attention (Weissman et al., 2006; Li et al., 2007; Eichele et al., 2008); its suppression is correlated with better memory enconding (Daselaar et al., 2004, 2009; Otten and Rugg, 2001) and increases with task difficulty (McKiernan et al., 2003; Singh & Fawcett, 2008). All these findings indicate that worst task performance is associated with greater DMN activation, but they do not define the process that this network mediates.

DMN activations were found during diverse mental scenarios, such as autobiographical memory retrieval (Andreasen et al., 1995; Svoboda et al., 2006), future envisioning (Partiot et al., 1995; Okuda et al., 2003; Szpunar et al., 2007; Addis et al., 2007; Botzung et al., 2008), inference of the mental state of others (theory of mind) (Fletcher et al., 1995; Saxe and Kanwisher, 2003; Saxe et al., 2004; Rilling, 2004) and reasoning about moral dilemmas (Greene et al., 2001; Greene and Haidt, 2002). Although these different mental contents diverge in temporal focus and personal perspective, they all converge in similar core processes: in each instance, the subject is required to simulate an alternative perspective to the present (Buckner and Carol, 2007). The construction of mental simulations and self-referential processing constitutes an important adaptive function, since it allows individuals not only to prepare for upcoming events (Baird et al. 2012, Smallwood 2013) but also to form a sense of self-identity and continuity across time (Prebble et al., 2013).

1.2.2.1.2 | Task-positive networks

Apart from the previously discussed deactivations observed in DMN regions, attention-demanding tasks also induce activity increases in numerous regions. Many of these activations are task-specific and localized in sensory and motor cortices. However, several frontal and parietal regions consistently exhibit activity increases, independently of the task performed. This set of brain regions, known as the task-positive network (TPN), includes parts of the dorsal attention network (DAN), ventral attention network (VAN) and frontoparietal control network (FPCN).

DAN is a brain system that comprises the posterior prefrontal cortex, the inferior precentral sulcus and the superior parietal lobule (Corbetta and Shulman, 2002). This network supports visuospatial processing and is therefore typically associated with focused attention on external stimuli (Corbetta and Shulman, 2002). Specifically, DAN seems to select sensory stimuli based on internal goals or expectations (goal-directed/top-down attention). DAN has been found anticorrelated with DMN not only during tasks but also during rest (Fox et al., 2005). This dynamics is altered in psychopathological disorders such as schizophrenia and depression (Whitfield-Gabrieli and Ford, 2012; Anticevic et al., 2012). The patterns of anticorrelation between DMN and DAN indicate that two modes of information processing may exist: one focused on information extracted from sensory channels, supported by DAN, and another one detached from the external environment that allows mental explorations to occur, supported by the DMN (Andrews-Hanna et al., 2014).

VAN is a right lateralized network which core regions include the temporoparietal junction and the ventral frontal cortex, including parts of the middle frontal gyrus, inferior frontal gyrus, frontal operculum and anterior insula (Corbetta and Shulman, 2002). This system detects behaviourally relevant stimuli in the environment, especially when unexpected (stimulus-driven/bottom-up attention), and interrupts DAN's ongoing activity in order to direct attention to such salient events. During attention-demanding tasks, VAN must therefore be suppressed to prevent reorienting to distracting events. A set of VAN regions has been referred in the literature as aggregated or closely adjacent to the salience network (SAL), comprised by anterior insula and dorsal ACC (Seeley et al., 2007) and associated with detection of behaviourally relevant (salient) stimuli.

The FPCN plays an important role in executive control of attention (Dosenbach et al., 2006; Vincent et al., 2008; Banich, 2009; Niendam et al., 2012; Cole et al., 2013). Its regions include dorsolateral prefrontal cortex, anterior IPL, dorsal ACC, frontal operculum/anterior insula, precuneus and posterior inferior lateral temporal cortex (Yeo et al., 2011; Vincent et al., 2008). Interestingly, FPCN anatomy is interposed between DMN and DAN (Power et al., 2011; Yeo et al., 2011; Spreng et al., 2010), and a recent study showed that while DMN and DAN share little positive functional connectivity with each another, the FPCN exhibits a high degree of interconnectivity with each of these networks (Spreng et al., 2013). These results are consistent with the idea that FPCN mediates the dynamic balance between these two

opposing networks, through their selective activation and suppression. This hypothesis is supported by fMRI data collected from subjects during performance of different planning tasks: visuospatial planning engaged the DAN and autobiographical planning engaged the DMN, as expected, while both engaged the FPCN, which was found functionally coupled with DMN during the autobiographical task and with DAN during the visuospatial task (Spreng et al., 2010). The involvement of the FPCN in the dynamics of DAN and DMN has been found in certain forms of self-regulation (Hare et al., 2009; Peters and Büchel, 2010), emotion regulation (Ochsner et al., 2012; Buhle et al., 2013), memory suppression (Depue et al., 2007) and perceptual decoupling (Christoff et al., 2009). Therefore, the aim of FPCN may be the mediation of internally and externally directed cognition.

A set of FPCN regions is often described as a separate network, the cinguloopercular (CO) network. This network was identified by Dosenbach et al. (2006), in a study that sought to identify the areas which activity was consistently maintained during a variety of tasks (10 tasks, including letter identification, reading, object naming, matching and judgment). According to their results, the regions that form the core of the task-set system are the dorsal ACC/medial superior frontal cortex and the left and right anterior insula/frontal operculum. One year later, Dosenbach et al. used graph theory regions interactions and suggested the presence of two distinct task-control networks: a frontoparietal, which included dorsolateral prefrontal cortex and intraparietal sulcus, and a cinguloopercular, comprised by dorsal ACC/medial superior frontal cortex, anterior insula/frontal operculum and anterior prefrontal cortex. They proposed that, while the first network might initiate and adapt control on a trial-by-trial basis – since its regions typically show transient activations related to task set initiation and error signalling –, the second would probably control goal-directed behaviour through the stable maintenance of task sets. In a posterior study, Sestieri et al. (2014) verified that CON regions displayed sustained signals during extended periods of not only a perceptual but also a memory task, thus supporting Dosenbach's hypothesis. Moreover, these results contest the hypothesis that CON corresponds to the salience network (Menon and Uddin, 2010), that facilitates the detection of behaviourally relevant (salient) stimuli.

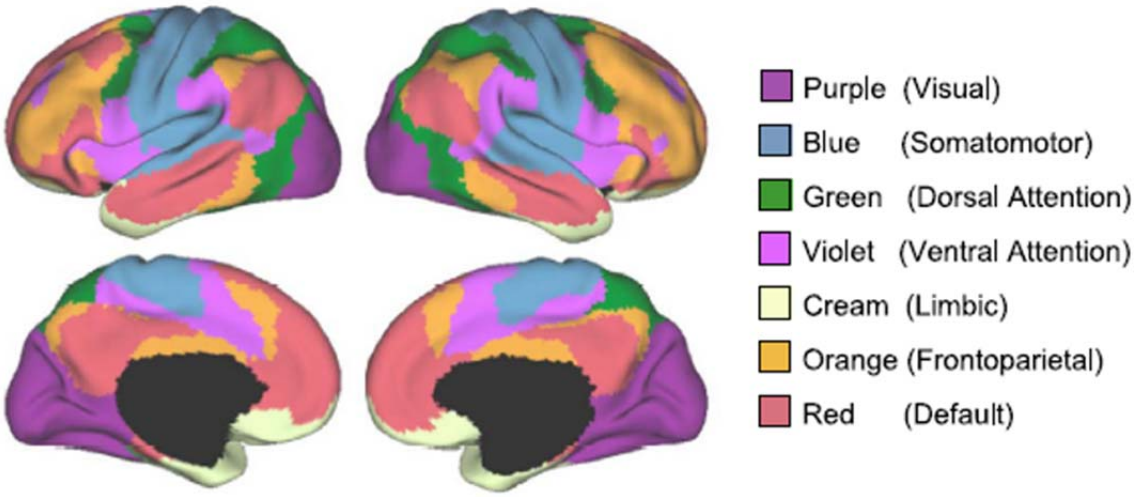

Figure 1 – Parcellation of the human cortex derived by Yeo et al. (2011) using resting-state functional connectivity MRI. Seven of the functional networks of the human brain are represented, including the main four networks discussed (DAN, VAN, FPCN, DMN) and three other commonly described networks (visual, somatomotor and limbic).

1.2.2.2 | Functional connectivity patterns

The intrinsic and extrinsic (task-evoked) architectures of both DMN and TPN seem almost identical (Smith et al., 2009). Both of these networks exhibit strong intranetwork correlations not only in resting-state but also during task performance (Mennes et al., 2012; Cole et al., 2014). This observation is consistent with the persistence of another relation in both task and rest states: the anticorrelation between DMN and TPN regions (Greicius et al., 2003; Fox et al., 2005), which strength was found increased during task performance and associated with better cognitive function, not only in external attention tasks (Kelly et al., 2007; Spreng et al., 2010) but also in a working memory task (Hampson et al., 2010).

1.2.2.2.1 | DMN functional connectivity

Although DMN regions usually exhibit task-induced deactivations, performance on a working memory task was found positively correlated with the strength of functional connectivity between medial frontal gyrus/ventral ACC and PCC (Hampson et al., 2006), two DMN hubs, suggesting intraconnectivity in this network may be increased during tasks. Wang et al. (2012) extended this analysis by computing FC between each DMN region pair and observed a predominantly intensified intra-DMN FC (except among bilateral PCC and left angular gyrus) during a visual semantic-matching task, compared to rest. Identical results were

obtained by Gao et al. (2013) in an external visual classification task, by Goparaju et al. (2014) in a visual motion task and by Repovs and Barch (2012) in a working memory task. However, other studies present opposing evidence; Fransson et al. (2006), for instance, found a substantially task-induced attenuation in the level of correlational activity in the DMN during a working memory task, as well as Hasson et al. (2009), during listening tasks. The discrepancy between these results may be due to the variability of methods and tasks specificities, which may induce different dynamic network reorganizations, as well as the regions used, for instance ACC is considered as a DMN region by some and as a task-positive region by others, partly because areas boundaries are not consistent across parcellation schemes.

Several task-positive regions have been found correlated with DMN not only in autobiographical tasks (Spreng et al., 2010), as referred in the previous subsection, but also during external attention demanding tasks. Wang et al. (2012) reported increased FC between DMN and frontoparietal regions during a simple attention task (visual semantic-matching), while Gao et al. (2013) identified bilateral insula/inferior frontal cortex, ACC and middle cingulate gyrus as regions with enhanced correlational activity with DMN, in an external visual classification task. Two of these regions (dorsal ACC and anterior insula), sometimes referred as a task control network, or salience network (SAL), are related to salience detection and processing and were found more coupled with DMN during a selective attention task (Elton and Gao, 2013).

Wen et al. (2013) explored the interaction between DMN and SAL in a visual spatial attention task and causal influences were found in both directions. The influence of SAL on DMN activity was interpreted as a mechanism to facilitate inhibition of task-independent thoughts through DMN suppression, while the inverse causal influence was found negatively correlated with behavioral performance and associated with less elevated BOLD activity in the target regions (anterior insula and dorsal ACC).

Analysis of functional connectivity between DMN and task-relevant regions have reported a decreased correlation between them in task contexts. Hasson et al. (2009), for instance, observed a reduced connectivity between DMN regions and lateral temporal cortex during a listening comprehension task, while Wang et al. (2012) reported lower correlational activity

between DMN and occipital areas during a semantic-matching task that involved visual processing.

1.2.2.2.2 | TPN functional connectivity

Each of the task-positive networks, including DAN, VAN, FPCN and CON, have been largely identified in resting-state fMRI connectivity studies (Fox et al., 2006; Yeo et al., 2011; Power et al., 2011; Lee et al., 2012), revealing that, as previously mentioned, the network organization of the brain is persistent across different states. Relationships between regions of these networks have been examined in several studies.

As referred in the previous subsection, Spreng et al. (2010) observed increased coupling between FPCN and DAN during a visuospatial planning task and between FPCN and DMN during an autobiographical planning task. Similar results were obtained by Gao and Lin (2012) during a sequential finger tapping task (which activated DAN) and rest.

Considering evidence suggesting that FPCN is functionally heterogeneous, including a control network (CON) and a salience network (SAL), Elton and Gao (2013) investigated CON and SAL task-dependent changes in connectivity. During a selection attention task, CON increased correlation with visual cortex regions associated with DAN, while SAL coupling with DMN was found enhanced. This last result is consistent with Gao et al. (2013) and Wen et al. (2013) findings, mentioned in the previous subsection. In fact, Sridharan et al. (2008) found a casual connectivity pattern showing that SAL and CON regions played a critical and causal role in switching between the central-executive network and DMN, during a visual attention "oddball" task and a task-free resting-state, respectively. Chiong et al. (2013) and Goulden et al. (2014) confirmed these results using different methods. However, Sestieri et al. (2014) observed that CON flexibly linked with DAN or DMN regions during perceptual or memory search, respectively, in opposition to Elton and Gao (2013) findings. This discrepancy may result from different methodologies and task paradigms.

Wen et al. (2012) assessed FC between DAN and VAN during a cued visual spatial attention task and found that heightened connectivity from DAN to VAN was correlated with improved task performance, while stronger influences from VAN to DAN were associated with worst performance. In the light of these findings, the authors suggested that signals from DAN to

VAN might suppress and filter distractors, whereas signals in the reverse direction would interrupt the attentional set maintained by DAN to enable attentional reorienting.

1.2.2.3 | Global functional properties

Several task-related changes have been found in global functional properties of the brain.

Wang et al. (2012) observed a higher local efficiency and lower global efficiency during a visual semantic-matching task, compared to rest. Kida and Kakigi (2013) found a reduced functional segregation in a cue-target attention task, supporting Wang and colleague's findings. Goparaju et al. (2014) used graph theoretical measures such as degree, betweenness centrality and path length to show that performance in a visual motion task induced stronger inter-regional connections but a less efficient system globally, again supporting Wang results. However, opposing evidence was found by Di et al. (2013), which results suggest a more efficient global information transmission and between system integration during task performance, since they found greater global efficiency, smaller mean clustering coefficient, and lower modularity in coactivation networks, compared to resting-state networks.

Elton and Gao (2015) used an external visual classification task to study FC variability and found that this measure demonstrated significant task-related decreases at the regional, network and system levels, which were greater for between-network interactions than within-network connections. Moreover, the degree of task-induced decreases in FC variability was significantly correlated with task performance accuracy, supporting the hypothesis that this measure is partly underpinned by unconstrained mind wandering.

2 | METHODS

2.1 | Anatomical data

We used an anatomical connectome with 90 brain regions, defined by the AAL parcellation scheme (Tzourio-Mazoyer et al. 2002), provided by Dr Joana Cabral (Researcher at the Depatment of Psychiatry, University of Oxford). The methodology used to acquire and process the fMRI data to obtain the final connectome is described in Cabral et al. (2012). The brain network was constructed using diffusion tensor imaging (DTI) from 21 healthy adults; for each subject, a 90x90 weighted connectivity matrix C was derived using the methodology from Gong et al. (2009). Each element of the connectivity matrices, C_{np}, represents the connectivity strength from node n to node p and is proportional to the number of fibres incoming to region n and to the size of that region, since the activity in each region is sensitive to the number of incoming axons per neuron. Therefore, the total number of incoming white matter tracts was divided by the relative size of the target region p, resulting in a non-symmetric connectivity matrix. As the dynamical model of one region already takes into account the effects of its internal connectivity, the connection of a region to itself was set to zero in the connectivity matrix. These 21 connectivity matrices were averaged across subjects resulting in a single coupling matrix, representative of the human connectome. The distance between each pair of regions, D_{np}, was taken as the Euclidean distance between the corresponding centres of gravity in the AAL template.

A geometrical view of the used connectome is depicted in Figure 2A. The anatomical connectivity matrix represented in Figure 2B, arranged so that homotopic regions are symmetric in respect to the matrix centre, allows to observe that, as expected, intrahemispherical connections (represented in the top left and bottom right matrix quarters) are more numerous than the interhemispherical ones (represented in the top right and bottom left matrix quarters). Instead of showing a random structure, this arrangement unveiled the existence of clusters, of a small-world organization of brain networks previously noted by Bullmore and Sporns (2009). Figure 2C presents the matrix of distances of existing connections, i.e., its elements correspond to the Euclidean distance between each pair of regions that share an anatomical connection.

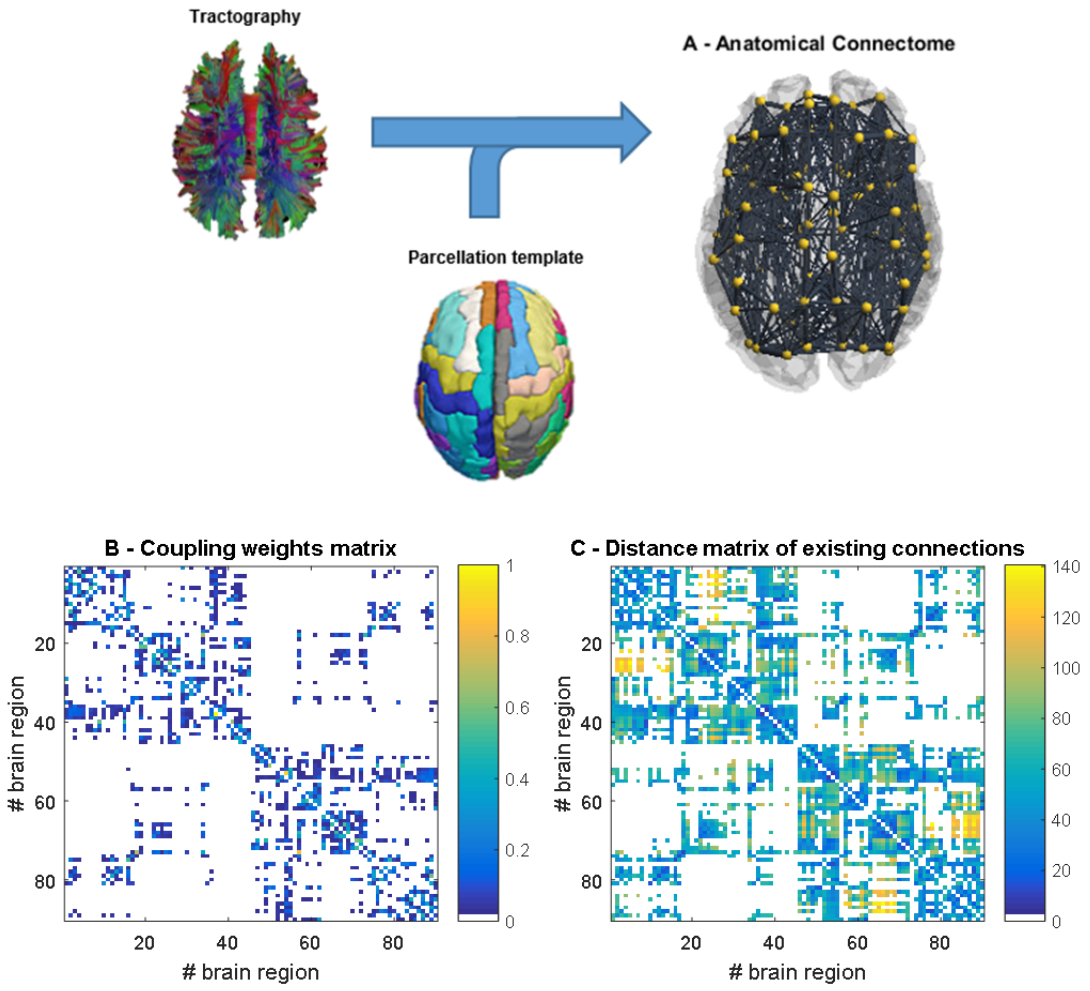

Figure 2 - Anatomical connectome used in the model. (A) Spatial representation of the anatomical connectome. Yellow spheres represent individual regions (nodes in the network). (B) Matrix of connections between regions. Connection weights are proportional to the number of fibres. (C) Distance between regions in mm, given as the Euclidean distance between centres of gravity. The list of brain regions and corresponding indexes is reported in A.1 Table1.

2.2 | Neural dynamics model

Resting-state brain activity was simulated using a computational model inspired in the Kuramoto model, which describes the dynamics of coupled oscillators (Acebron, 2005; Kuramoto 1984). Kuramoto model variations have been used to simulate synchronization phenomena in different fields, including biological systems (Pikovsky et al., 2001; Strogatz 2003) and, more recently, large-scale brain dynamics (Breakspear et al., 2010; Cabral et al., 2011; Kitzbichler et al., 2009; Yan and Li, 2013). Reducing the dynamics of a brain region to a phase-oscillator involves a high degree of abstraction, but this approach is supported by evidence suggesting neural populations' activity produce moderately synchronized oscillations, particularly in the gamma frequency range (Bartos et al., 2007; Borgers and Kopell, 2003; Brunel, 2000; Brunel and Wang, 2003). In fact, Cabral et al. (2011) showed that weakly coupled gamma-band oscillators with a complex topology, like the brain, exhibited a complex synchronization behaviour such as multistability and metastable cluster synchrony, under certain parameter conditions, mimicking some of the properties of brain functional dynamics.

Self-sustained oscillations exhibited by neural populations result from the balanced activity of excitatory and inhibitory neurons, which firing rates describe a closed periodic trajectory in phase space – a limit cycle. The dynamics of each population may thus be approximated by a single variable, the angle or phase on this cycle. Therefore, the population itself can be represented as a periodic self-sustained phase-oscillator, and the brain as a network of these oscillators.

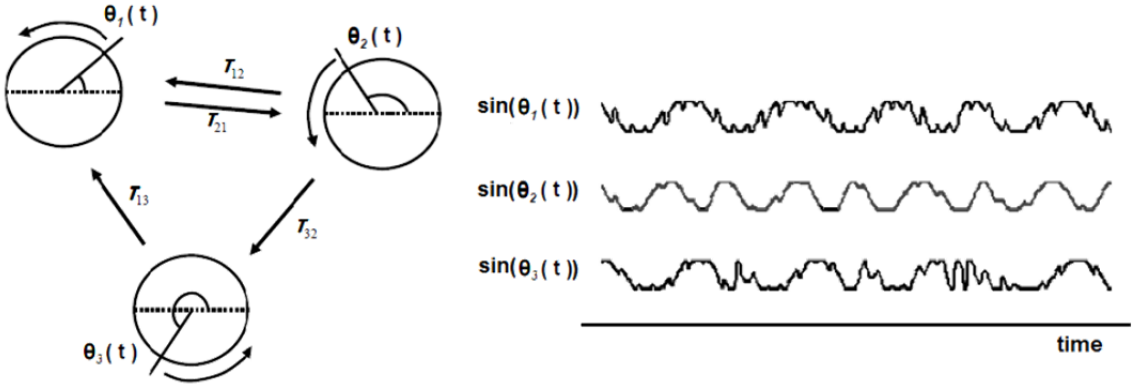

Figure 3 – Graphical representation of three interacting oscillators with delayed coupling, where the angle on the circle represents the phase on the limit cycle, and three time series obtained from $\sin(\Theta_n(t))$. From Cabral et al. (2011)

The phase of brain region n (node n), denoted by Θ_n, obeys the following dynamical equation:

$$\frac{\partial \theta_n}{\partial t} = w + k\sum_{p=1}^{N} C_{np}\ \sin\left(\theta_p\left(t - \tau_{np}\right) - \theta_n\right), n = 1, \ldots, N.$$

w is the natural frequency of each node on its limit cycle, when uncoupled; k is the global coupling that uniformly scales all connectivity weights; N is the number of nodes in the network; τ_{np} is the time delay and C_{np} is the coupling strength from node p to node n.

This equation differs from the classic Kuramoto model in two aspects. Here the natural frequency is identical for all oscillators, while in the original model natural frequencies had a distribution with a given probability density; this reduction was made to minimize the number of parameters, and was previously shown not to significantly affect the network dynamics in this model (Cabral et al., 2014). The other modification is the incorporation of time delays, which allows the simulation of delayed communication between neural populations caused by the finite conduction speed of axonal fibres, thus improving the neurobiological plausibility of the model. The delay, τ_{np}, is proportional to the distance D_{np} and to the conduction velocity v (assumed homogeneous, for simplicity (Deco et al., 2009; Ghosh et al., 2008)), such that: $\tau_{np} = D_{np}/v$.

2.1.1 | Resting-state simulation

Resting-state activity was initially revealed by slow fluctuations (<0.1 Hz) of the BOLD fMRI signal (Biswal et al., 1995; Gusnard and Raichle, 2001), which lead to the identification of large-scale resting-state networks (RSNs), including DMN. A counterpart of these slow fluctuations in neural activity are the slower power fluctuations of local field potential (LFP) gamma frequency oscillations. Importantly, Basar-Eroglu et al. (1996) suggested the existence of a distributed system of gamma (40 Hz) generators in the brain and an interpretation of gamma rhythms as universal functional building blocks. In agreement with these predictions, Cabral et al. (2011) results show that gamma-band oscillators can serve as fundamental units to build a complex multi-frequency dynamics. Therefore, in the computational model used here, the natural frequency of the oscillators was set within the gamma frequency range to 40 Hz.

The network was defined using the previously described structural connectivity: the anatomical connectivity matrix C (normalized so that the mean strength is 1), and the distance matrix D. The only free parameters are then the global coupling k and the time delay τ, since it depends on the variable parameter v. The values of these two parameters were selected regarding several aspects that will shortly be discussed. Phases were initialized randomly and the initial 200 s were discarded to remove initial transient dynamics. The system of N coupled delay differential equations was numerically integrated using an Euler scheme with a time step of 0.1 ms. All calculations were performed using MATLAB (http://mathworks.com).

2.2.2 | Characterization of the network dynamics

To characterize the dynamics of the whole network, Kuramoto (1984) derived an order parameter that measures the phase uniformity among nodes, given by R(t):

$$R(t)e^{i\phi(t)} = \frac{1}{N}\sum_{n=1}^{N} e^{i\theta_n(t)}$$

The degree of synchrony is given by the modulus of the order parameter, R(t). If the network is too weakly coupled (below the critical coupling, k_c), all nodes (initialized with random phases) continue firing independently and $\lim_{t\to inf} R(t) = 0$; in this case, the system is said to be in a stable asynchronous (or incoherent) state. On the opposite side, if the coupling is higher than k_c, the system will tend to a fully synchronized state and $\lim_{t\to inf} R(t) = 1$. If the network has a non-homogeneous connectivity structure, forming clusters of highly connected nodes, like the brain, then modular structures of synchronized nodes will progressively emerge in hierarchical order, until global synchronization is reached.

The model used, on the contrary, exhibits intrinsic instabilities introduced by time delays, when this parameter is defined in a certain range. In that case, the system displays multiple meta-stable equilibria (Strogatz, 2001), similar to brain dynamics. Therefore, to characterize the dynamics of this system, we used the mean of the *order parameter*, $\bar{R}$, an index of the global synchronization level, and its standard deviation, σ_R, related to the metastability level of the network (Shanahan, 2010), as previously done by Cabral et al. (2011).

In order to obtain a dynamics that reproduces resting-state brain activity, it is therefore necessary to determine the parametric conditions under which multistability occurs. As previously referred, since C_{np}, D_{np} and w are fixed, the only two free parameters are the global coupling k and the time delay τ. Simulations of 300 s for a range of global coupling strengths and mean delay were then performed.

2.3 | Simulated BOLD signal and functional connectivity

To relate the simulated neural activity of each node to the BOLD signal, we used the Balloon-Windkessel hemodynamic model proposed by Friston et al. (2000, 2003), assuming that firing rate variations of neural populations underlie the BOLD signal. In the model, fluctuations of each node can be described by a periodic function of the phase, such as the sine (Figure 3); therefore, the simulated neural activity (firing rate) of node n may be given by: $r_n(t) = r_0 \sin(\theta_n(t))$, where r_0 is the fixed amplitude of the fluctuations.

To perform a comparison between simulated and empirical FC, these simulated BOLD signal were band-pass filtered in 0.25 Hz to remove small and non-physiological high frequency components that can induce spurious correlations. To reduce computational complexity, we down-sampled the BOLD time-courses at 0.2-second resolution. Finally, to extract the simulated functional connectivity (FC), we computed the Pearson correlation between the BOLD signals of each pair of regions. This measure provides a simple characterization of temporal interactions between brain regions.

To evaluate the performance of the model, the simulated functional network was compared with an empirically derived FC matrix. This matrix was derived using the AAL parcellation scheme from BOLD signals acquired from 16 healthy subjects, during rest, and was provided by Dr Joana Cabral from the Department of Psychiatry, University of Oxford. Simulated and empirical FC matrices were compared using Pearson correlation.

2.4 | Simulation of cognitive states

To simulate different brain modes – the rest and the task state –, two approaches that implicated the manipulation of the connectivity matrix were tested.

In the first method, we followed the methodology from Hellyer et al. (2014), increasing the efferent connection strengths of regions typically active during performance of tasks. If a given brain region is more active, this is assumed to result in increased influence over connected regions. Therefore, to simulate the task state, TPN regions (bilateral frontal gyrus, inferior frontal gyrus pars opercularis and superior parietal lobule) were increased by multiplying factors of 2, 4 and 8 and the corresponding simulated data were denominated 'Tasks 1, 2 and 3', respectively. The baseline simulation (with no alterations in structural connections) was designated as 'Rest'. We thought this was the best definition of resting state as the model parameters were set so that the model would reproduce functional data from resting state MRI scans. As a control for this methodology, we also performed a similar set of simulations after increasing the same number of efferent connections of a different network, the DMN.

In the second approach, we were inspired by the work of Wen et al. (2012), which found that an enhanced performance during tasks was associated with stronger Granger causal influences from DAN to VAN. On the contrary, stronger Granger causal influences from VAN to DAN were associated with degraded performance. Therefore, we attempted to simulate a task state by increasing the strength of connections from DAN to VAN by factors 2, 4 and 8. The resulting data were designated as 'Task 4, 5 and 6', while the baseline is denominated 'Rest', as with the previous method. We then performed Granger causality analysis on BOLD signals from these networks regions in order to verify if we could indeed obtain the stronger influences from DAN to VAN observed by Wen et al. (2012) by magnifying the corresponding structural connections. This analysis was performed using the MVGC Multivariate Granger Causality Toolbox (Barnett and Seth, 2014). The order of the AR model was chosen to be 1 based on Akaike information criterion. To detect significant Granger causalities, an F-test was performed for each individual causality measure with a significance level of 0.05. A repeated-measures ANOVA was conducted to test the main effects of task. As with the previous method, we controlled for this methodology by performing a similar set of simulations after increasing the connections from DAN to another network, the DMN.

Different aspects were analysed in order to verify the validity of these methods, i.e., to evaluate if the simulated task signals exhibited similar properties to those extracted during performance of tasks in empirical experiments. We started by verifying if the variability of

functional connectivity decreased in simulated tasks, as it was demonstrated in an empirical study (Elton and Gao, 2015). The simulated task data that best exhibited this property from each method was selected to be further analysed using graph measures.

2.5 | Functional connectivity variability

To analyse the stability of each functional connection over time, we used the methodology of Elton and Gao (2015), which used a sliding window approach. We computed the Pearson correlation between each pair of BOLD signals, in each time window of 60 s, with an overlap of 2 s. The correlation coefficients were then converted to a normal distribution by Fisher Z-transform. With this procedure, we obtained a sliding window time series of correlations for each pair of regions. To calculate the variability of each of these time series, we used both the standard deviation and a coefficient of variation, defined as the standard deviation of each time series divided by the absolute value of its mean. Using repeated-measures ANOVA, we tested for the main effects of task and within-versus-between networks. The networks considered were DAN, VAN, DMN, Visual and Somatomotor, which are some of the most clearly characterized networks, in relation to their constitution (i.e., the brain regions that compose them) and to their behaviour in the rest and task states. The regions that were considered for each network are listed in Appendix A.I Table 2 and were based in Elton and Gao (2015), except for VAN (not included in Elton and Gao's list), which definition was based on Wen et al. (2012).

2.6 | Graph theory analysis

To compare the topology of the whole brain network in rest and task simulations, we computed several graph theoretical measures, using the Brain Connectivity Toolbox (Rubinov and Sporns, 2010). As recommended by the authors, all self-connections and negative connections were set to zero.

To assess the networks' connectedness, we computed the strength of each node, defined as the sum of all neighbouring link weights. The strength corresponds to the weighted variant of degree, which is the number of links connected to the node. Individual values of degree reflect the importance of the node, while the mean network degree is a measure of density.

The degree distribution, which shows how many nodes exist in the network with each degree, is a marker of network development and resilience.

Important nodes, known as hubs, tend to connect to numerous nodes, facilitate integration and play a key role in network resilience. Many measures of node centrality are based on the idea that central nodes participate in many short paths within a network, acting as important controls of information flow (Freeman, 1978). One of these measures, that we used, is the betweenness centrality, defined as the fraction of all shortest paths in the network that pass through the node.

To characterize how similar each region behaviour was in task and rest, we calculated the linear regression and variance of the relationship between task and rest networks. A slope of 1 with no variance would indicate that highly connected or central nodes in the rest network were equally connected/central in the task network.

Functional integration and segregation were also evaluated, using global and local efficiency, respectively. Global efficiency is the ability to rapidly combine specialized information from distributed regions; local efficiency is a similar measure but evaluated at the node level. These measures were evaluated using two processes. In the first approach, we used the intact weighted matrices, as for the previous measures. In the second process we binarized the matrices using a range of sparsity thresholds, from 10 to 50%, similarly to other studies (Cabral et al., 2012; Wang et al., 2012). While the first method has the advantage of reflecting not only the organization but also the magnitude of the connections (Elton and Gao, 2015), the second controls for the strength of the connections, ensuring that the measures obtained are only due to differences in topology and not in magnitude, and also eliminates weak and non-significant links that may represent spurious connections. Therefore, there is no consensus relative to the best method and we decided to use both.

3 | RESULTS

3.1 | Network dynamics

The global dynamics was assessed in the (τ, k) parameter space using two measures: the global synchrony level, estimated as the mean of the order parameter, and the global metastability level, evaluated as the standard deviation of the order parameter.

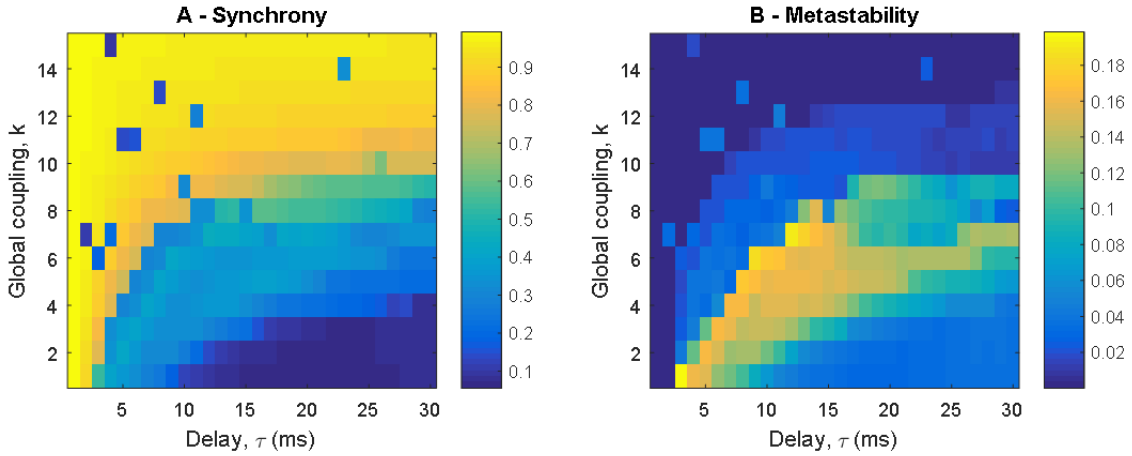

Figure 4 – Global dynamics in the delay and global coupling parameter space.

As shown in Figure 4, a division of the (τ, k) plane in three regions is evident. An area below the critical global coupling, characterized by an incoherent motion of the oscillators, has a global synchrony close to zero (Figure 5A), while the opposite zone exhibits an almost complete global synchrony (Figure 5C). An intermediate region presents partial synchrony and increased metastability (Figure 5B). In this third region, the model displays a metastable dynamics that allows the emergence of clusters that exhibit transient periods of synchronized and desynchronized activity.

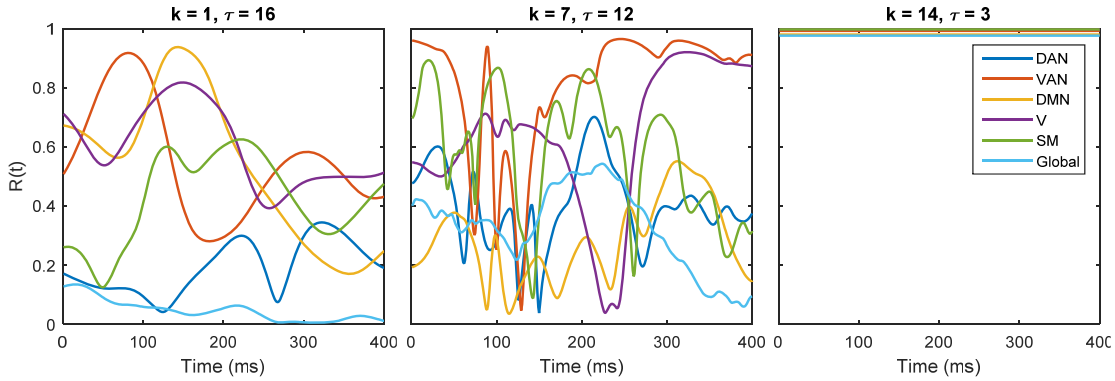

Figure 5 – Synchrony level (measured as R(t)) of the whole brain – 'Global' – and several known networks for different pairs of (k, τ) as a function of time.

3.2 | Working point selection

Three criteria were used to select the most appropriate free parameters (global coupling, k, and time delay, τ). Since resting-state activity is characterized by high metastability, which allows transient synchronization patterns to emerge, we identified the parametric conditions that maximized standard deviation of the order parameter, an index of the system's metastability (Figure 4B). The second criterion was the fit between simulated and empirical FC, estimated as the Pearson correlation between these two FC matrices (Figure 6A). The third criterion was the correlation between structural and functional connectivity (Figure 6B), known to be high in empirical studies (Honey et al., 2009).

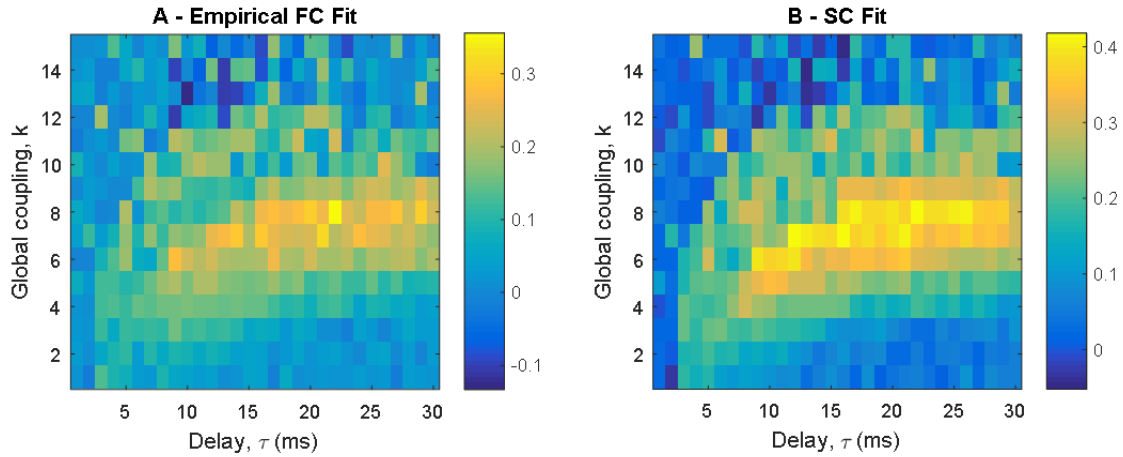

Figure 6 – Behaviour of the simulated FC in the parameter space. (A) Pearson correlation between the empirical and the simulated FC. (B) Pearson correlation between the structural connectivity and the simulated FC.

Considering all three criteria, we chose the working point (τ, k) = (12, 7). To assist in this decision, we computed the mean between the three matrices, resulting in the matrix shown in Figure 7.

The BOLD FC matrix corresponding to the selected working point is presented in Figure 7.

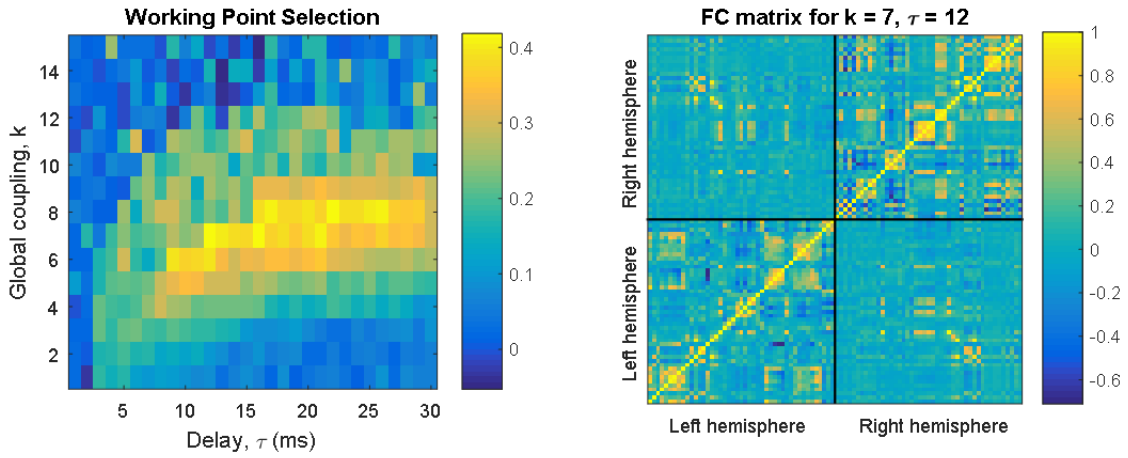

Figure 7 – (Left) Matrix of the mean of metastability, empirical FC fit and SC fit matrices. (Right) Simulated FC matrix in the selected working point, (τ, k) = (12, 7).

3.3 | Characterization of the simulated cognitive states

As previously referred, two methods were used in an attempt to simulate the task state: simulation of the activation of TPN regions by increasing the efferent structural connections of TPN regions and simulation of enhanced directed connectivity from DAN to VAN through augmentation of the strength of structural connections from DAN to VAN regions. For each of these methods, three task simulations were obtained, with different degrees of alteration. Tasks 1, 2 and 3 were obtained with the first method while Tasks 4, 5 and 6 derive from the second method. In this subsection, we report the results from analysis performed in these six simulated tasks data. The baseline simulation, to which the tasks are compared, is designated as 'Rest'.

3.3.1 | FC analysis

3.3.1.1 | First method: simulation of the activation of TPN regions

Results from FC analysis of the data obtained with the first method are displayed in Figure 8. A whole-brain change is evident in the three simulated tasks, not only in FC variability but

also in FC mean. There was a significant effect of task on the variability as measured by standard deviation ($F(3, 12006) = 976.25$, $P < 0.001$) and by the coefficient of variation ($F(3, 12006) = 3530.4$, $P < 0.001$), as well as on the mean ($F(3, 12006) = 3028$, $P < 0.001$). Post hoc testing using the Bonferroni method indicated the following significant differences: Task 1 > Task 3 > Rest > Task 2 for standard deviation; Rest > Task 3 > Task 2 for coefficient of variation and Task 2 > Task 3 > Task 1 > Rest for mean.

There was not a significant difference in standard deviation for within-network ($M = 0.2253$, $SD = 0.1183$) and between-network ($M = 0.2239$, $SD = 0.2473$) connections; $t(2806) = 0.1183$, $p = 0.05$. However, a significant difference was found in the coefficient of variation for within-network ($M = 0.1760$, $SD = 1.2008$) and between-network ($M = 0.3076$, $SD = 1.2004$) connections; $t(2806) = -2.2291$, $p = 0.05$. Similarly, a significant difference was detected in the mean for within-network ($M = 0.3523$, $SD = 0.6686$) and between-network ($M = 0.2781$, $SD = 0.5699$) connections; $t(2806) = 2.5609$, $p = 0.05$.

Lastly, the two-way repeated measures ANOVA did not reveal a significant within-versus-between by task interaction for neither standard deviation ($F(3, 2097) = 0.12304$, $P > 0.05$), nor coefficient of variation ($F(3, 2097) = 0.19246$, $P > 0.05$) nor mean ($F(3, 2097) = 0.14141$, $P > 0.05$).

Variability of sliding window FC

A

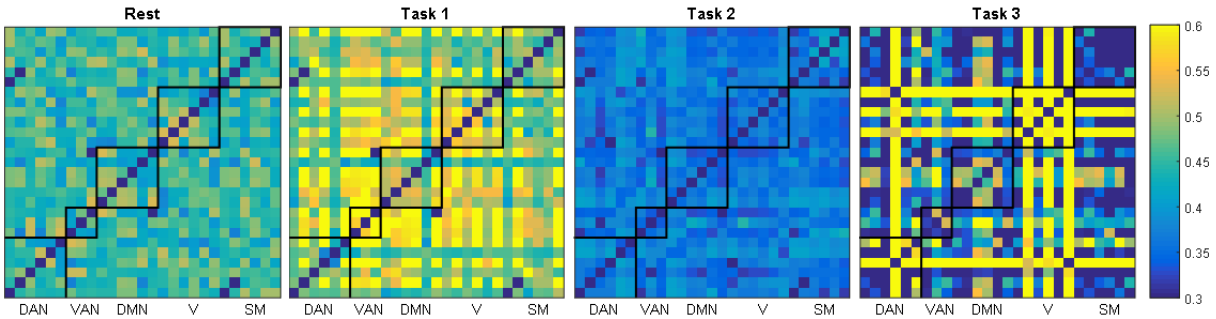

B

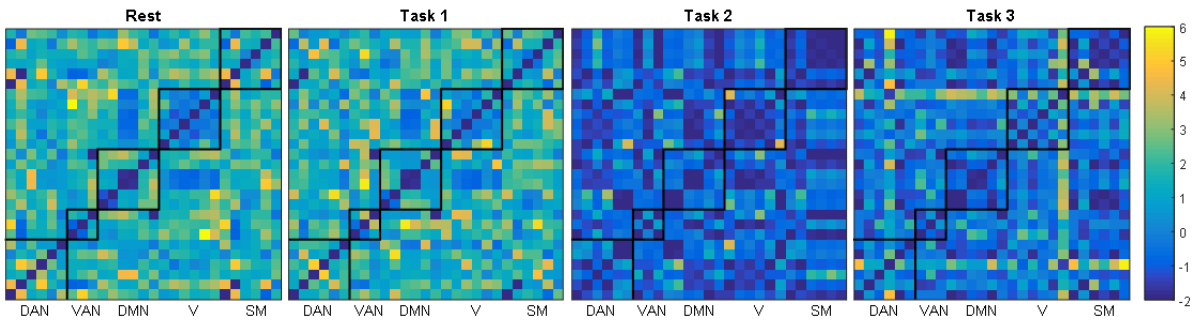

Mean of sliding window FC

C

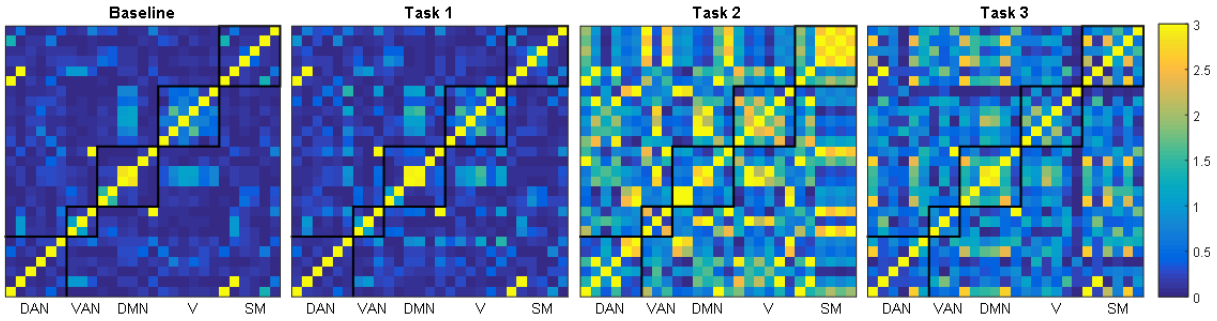

Figure 8 - Matrices of the effect of task on FC sliding window time series, including (A) standard deviation, (B) coefficient of variation and (C) mean. Within-network connectivities are underlined in black boxes.

3.3.2 | Second method: increased directed connectivity from DAN to VAN

Results of the Granger causality analysis are provided in Figure 9. An extensive causal flow originating from DAN to VAN regions is observable in Task 5. In 18 causal interactions from DAN to VAN, only one was significant in Rest, while 13 were significant in the simulated Task 5. Task 4 only presented 2 significant causal connections, while Task 6 exhibited 4.

These results indicate that the multiplication factor used in Task 5 simulation was the best to produce the desired effect of increased connectivity from DAN to VAN. We thus expected that Task 5 might yield good results concerning effective simulation of the task state.

A – Granger causality

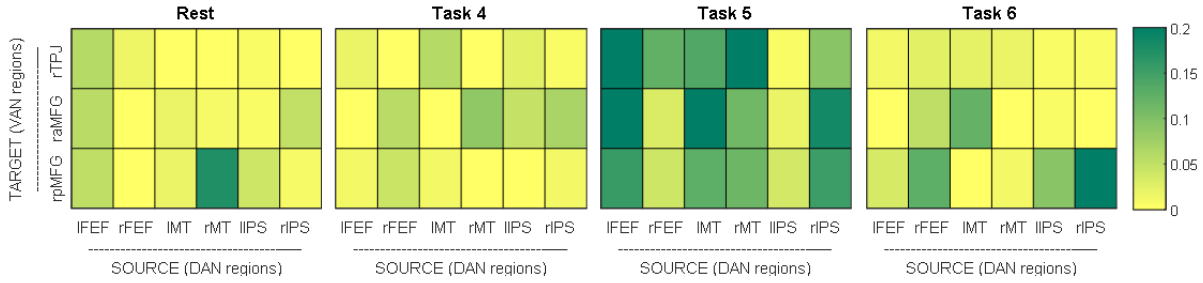

B – Significance of causal interactions

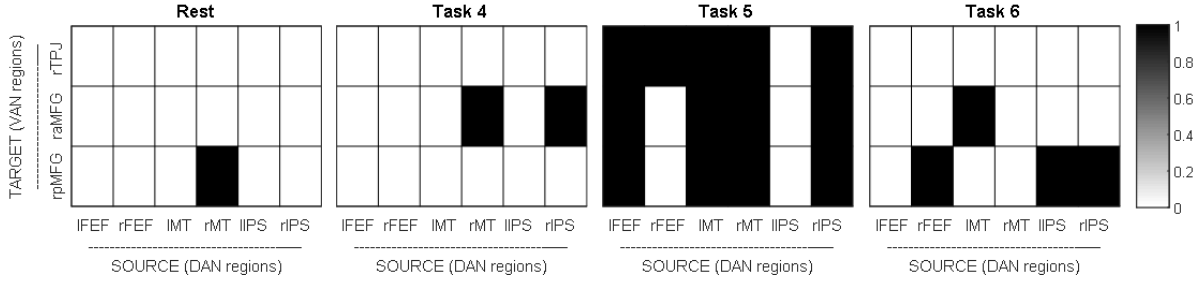

Figure 9 - Granger causality from DAN to VAN. (A) Granger causality values (F-values). (B) Significance of causal interactions. Let i denote the row index and j the column index. If the (i,j) cell is black, the Granger causal influences from i to j are significant at p = 0.05.

Results from FC analysis performed on the data obtained using the second method of task simulation are displayed in Figure 10. Once again, a whole-brain change caused by the SC alterations is noticeable, specifically in Tasks 4 and 5. Both standard deviation and mean matrices of Task 5 reveal a global increase, comparing to rest, while the coefficient variation matrix exhibits a global decrease, indicating that the variability in relation to the mean actually decreases. There was a significant effect of task on the variability as measured by standard deviation ($F(3,12006) = 457.01$, $P < 0.05$) and by the coefficient of variation ($F(3,12006) = 1622.8$, $P < 0.05$), as well as on the mean ($F(3,12006) = 2021.4$, $P < 0.05$). Post hoc testing using the Bonferroni method indicated the following significant differences: Rest > Task 4 > Task 5 for standard deviation and coefficient of variation and Task 5 > Task 4 > Rest for mean.

As with the first method, we did not find a significant difference between standard deviation for within-network (M = 0.2267, SD = 0.2306) and between-network (M = 0.2225, SD = 0.2272) connections; $t(2806) = 0.3797$, $p = 0.05$. However, a significant difference was found in the scores of coefficient of variation of within-network (M = 0.3270, SD = 1.0485) and between-network (M = 0.4901, SD = 1.0579) connections; $t(2806) = -3.1416$, $p = 0.05$. Similarly, a significant difference was detected between the mean of within-network (M = 0. 2445, SD = 0. 4789) and between-network (M = 0. 1638, SD = 0. 3125) connections; $t(2806) = 4.7126$, $p = 0.05$.

Similarly to the previous method, the two-way repeated measures ANOVA did not reveal a significant within-versus-between by task interaction for neither standard deviation ($F(3,12006) = 1.0864$, $P > 0.05$), nor coefficient of variation ($F(3,12006) = 0.52482$, $P > 0.05$) nor mean ($F(3,12006) = 1.9388$, $P > 0.05$).

Variability of sliding window FC

A

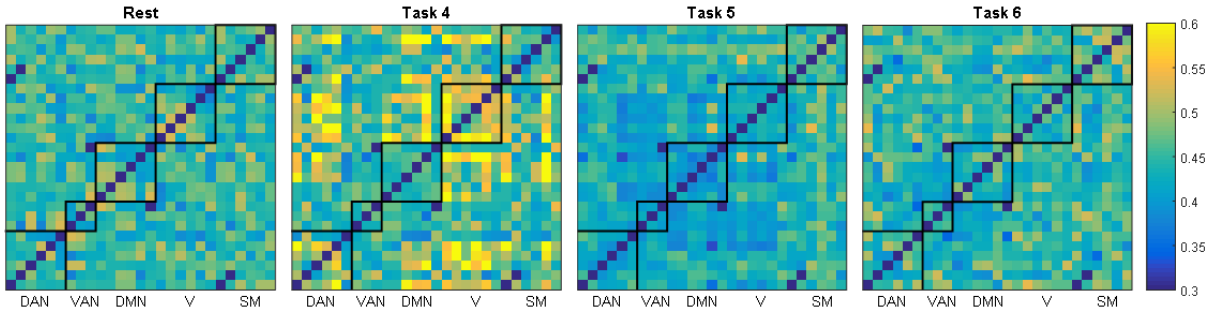

B

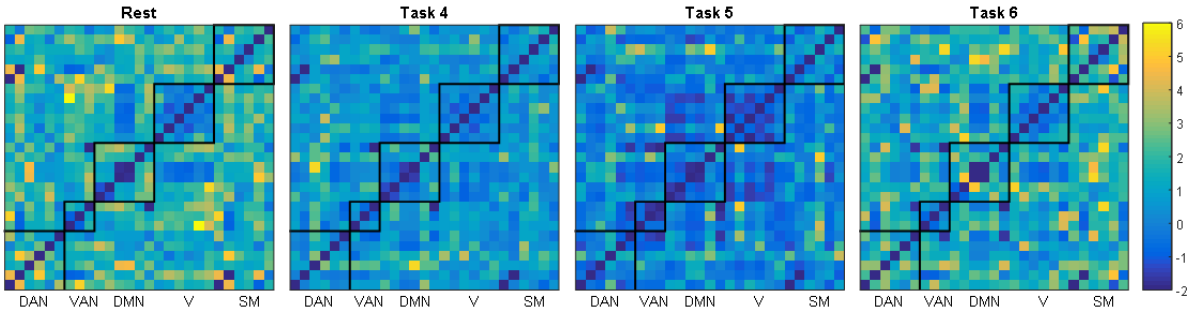

Mean of sliding window FC

C

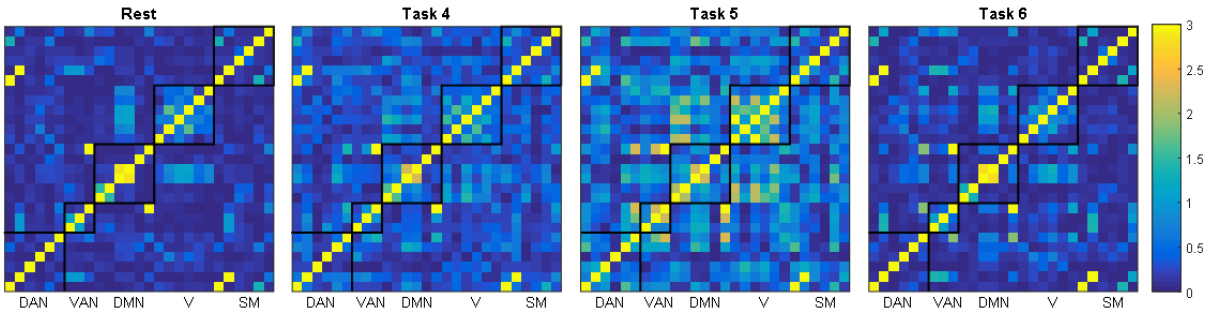

Figure 10 - Matrices of the effect of task on FC sliding window time series, including (A) standard deviation, (B) coefficient of variation and (C) mean. Within-network connectivities are underlined in black boxes.

As expected from Granger causality analysis, FC analysis revealed that from the tasks simulated using the second method, Task 5 was the best to reproduce a task state.

The analysis revealed significant alterations for several of the simulated tasks, with some of these exhibiting a higher FC variability and others a lower variability. A reduced variability

measured as both standard deviation and coefficient of variation was found in Tasks 2 and 5, therefore these were selected to the further analysis.

FC variability in the simulated tasks of control (resultant from the increase of strength of DMN efferent connections and of DAN → DMN connections) is presented in Appendix A.II.

Figure 11 illustrates the effect of Tasks 2 and 5 in the within and between-network FC of different networks. As can be observed, the effects in FC mean and variability are global, affecting almost uniformly every network considered. DMN, the network which activity is found decreased during rest, reduced the variability of its intra and extra-FC in Tasks 2 and 5, but also notably increased their strength.

Variability of sliding window FC

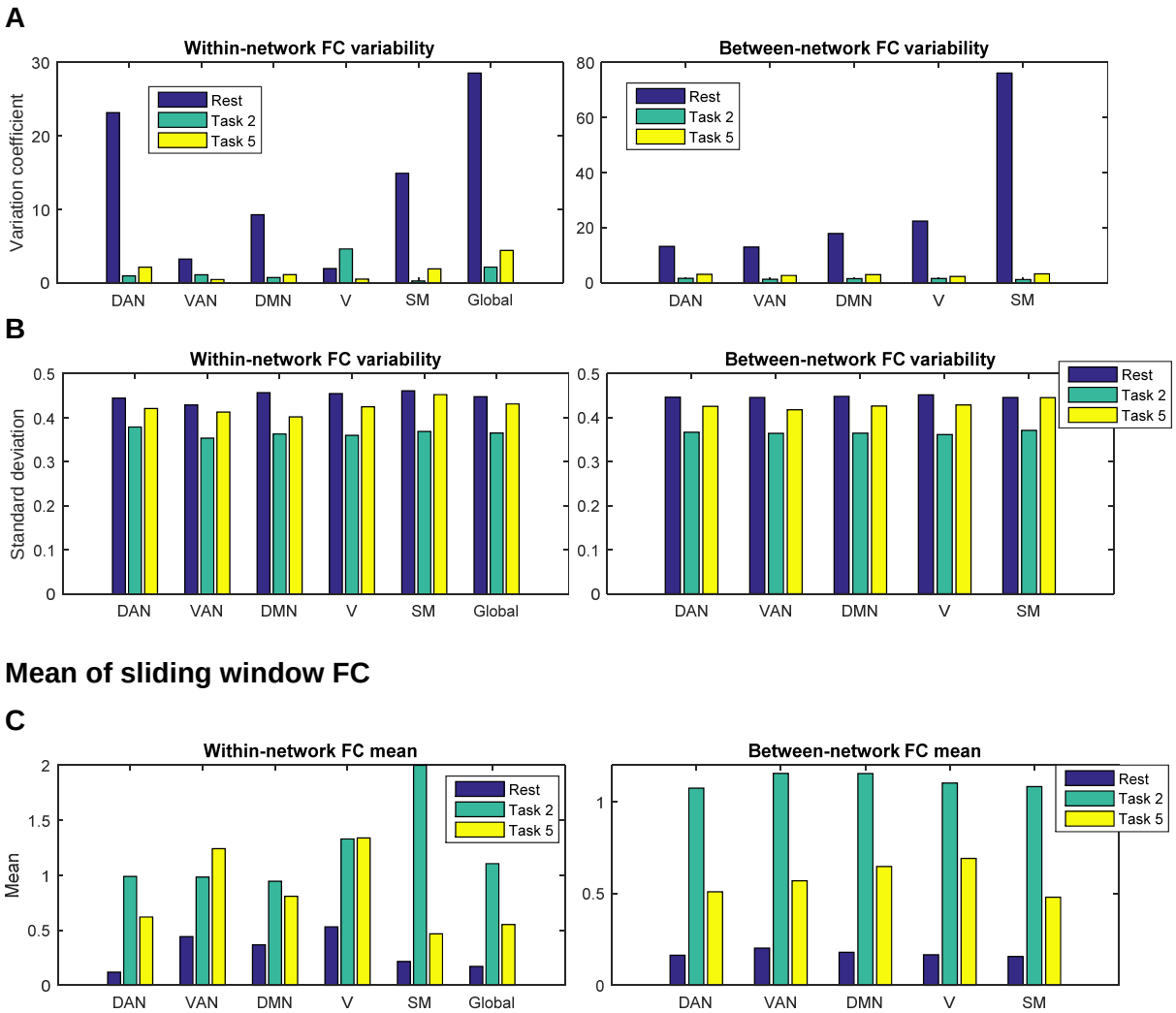

Mean of sliding window FC

Figure 11 – Bar plots of the effect of task on network FC sliding window time series, including (A) standard deviation, (B) coefficient of variation and (C) mean.

3.3.2 | Graph theory analysis

In this subsection, we present results of graph theory analysis that were performed on the Rest and Task 2 and 5 networks.

3.3.3.1 | Nodes strength

As expected from the previous FC analysis, we found a significant difference in the nodes strength for Task 2 (M = 66.9786, SD = 22.6100) and Rest (M = 9.4281, SD = 3.6053) networks; t(89) = -24.2374, p = 0.05. Similar results were obtained for Task 5 (M = 24.1987, SD = 9.8736); t(89) = -14.2798, p = 0.05. Consistent with these results, the tasks strength distribution was shifted higher, in comparison to rest (Figure 12), indicating a global increase in connectedness. However, both Rest and Task 5 present a normal distribution, while Task 2 does not.

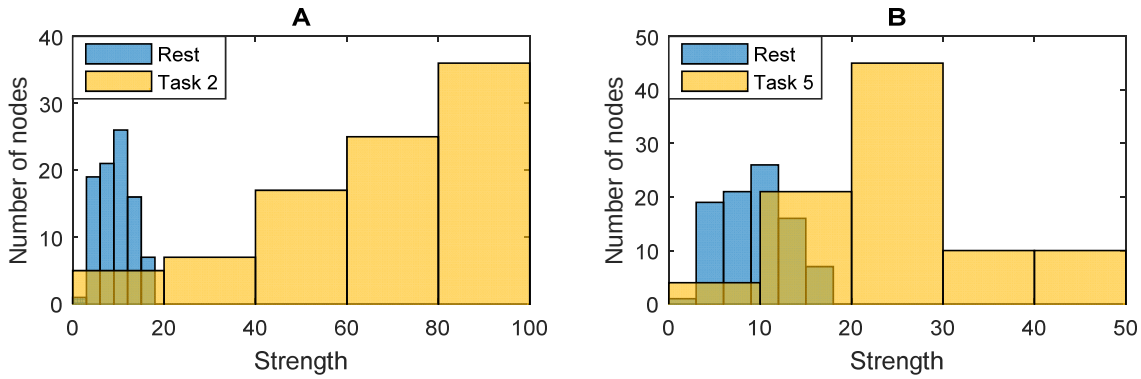

Figure 12 – Strength distribution of (A) Rest and Task 2 networks and (B) Rest and Task 5 networks.

The relationship between task and resting networks for strength is presented in Figure 13. A significant correlation between these two conditions was not found, suggesting that highly connected nodes in one condition are poorly connected in the other, and vice versa.

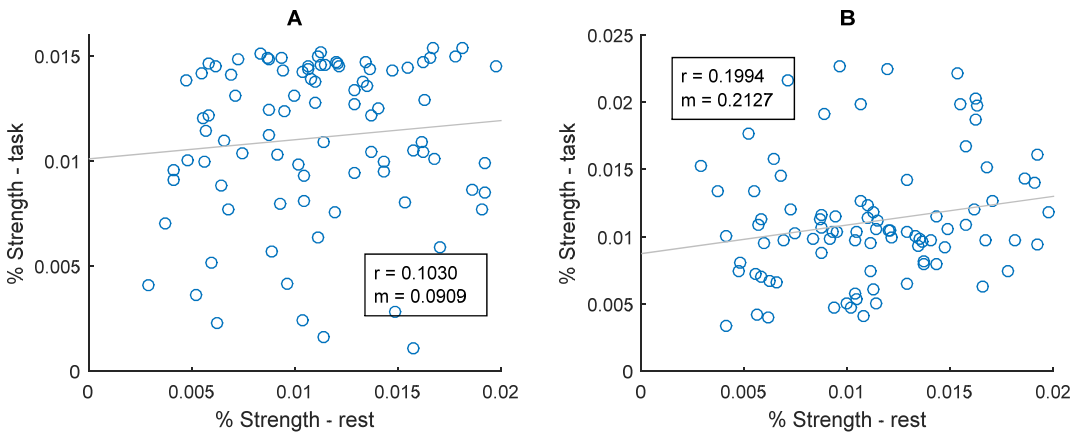

Figure 13 - Percent strength of each node of Rest and (A) Task 2 and (B) Task 5 networks, plotted against each other. Each blue circle represents a node, while the grey line represents the linear least-squared regression best-fit line, with the respective regression (r) and slope (m) values.

The variability of mean strength over time can be observed in Figure 14. There was a significant effect of task on the variance ($F(2,192) = 28.0568$, $P < 0.05$).

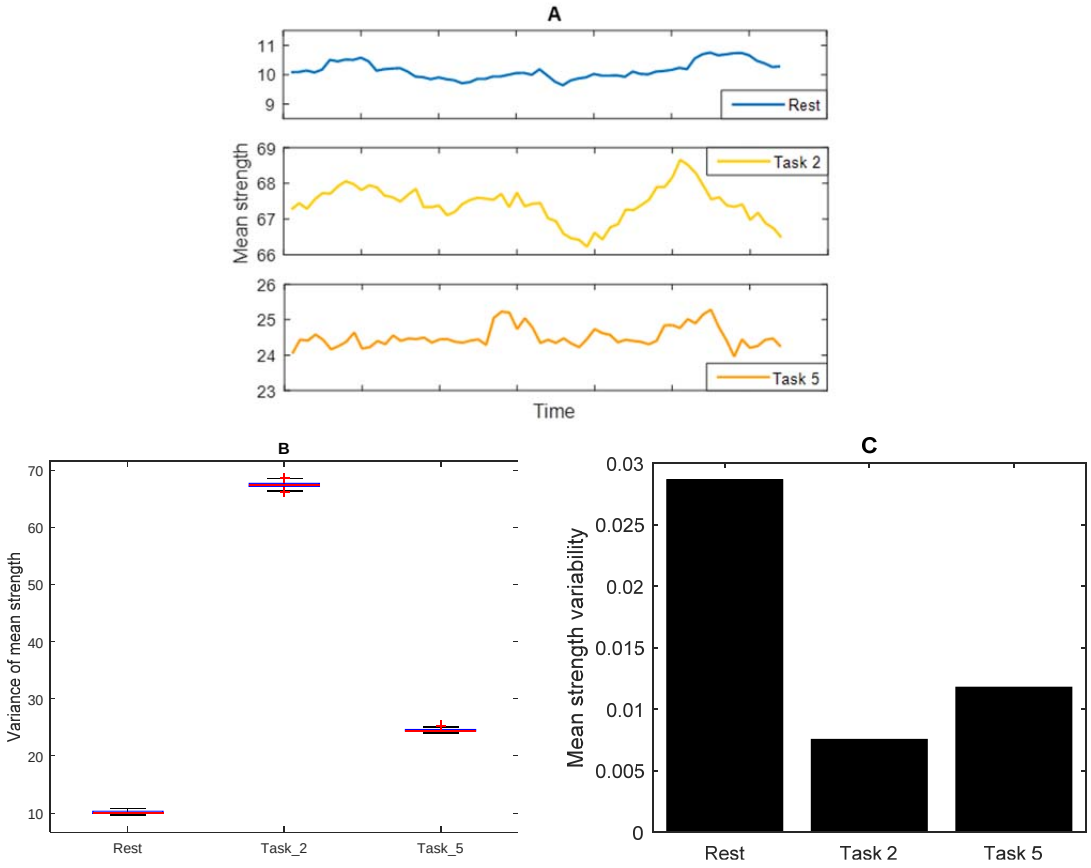

Figure 14 – Variability of mean strength of Rest, Task 2 and Task 5 networks. (A) Mean strength over time. (B) Bartlett's test for equality of variances. (C) Mean strength variability measured as the coefficient of variation of the mean strength over time.

3.4.2 | Centrality

The relationship between task and resting networks for betweenness centrality is presented in Figure 15. As with strength, a significant correlation between these two conditions was not found, suggesting that highly central nodes in one condition are not in the other, and vice versa.

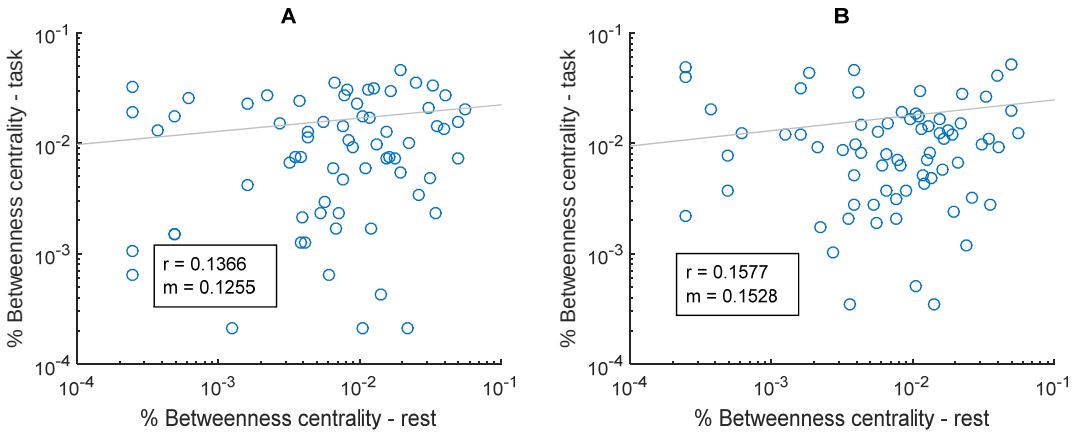

Figure 15 - Percent betweenness centrality of each node of Rest and (A) Task 2 and (B) Task 5 networks, plotted against each other. Each blue circle represents a node, while the grey line represents the linear least-squared regression best-fit line, with the respective regression (r) and slope (m) values.

The variability of mean betweenness centrality over time can be observed in Figure 16. There was a significant effect of task on the variance ($F(2,192) = 118.598$, $P < 0.001$).

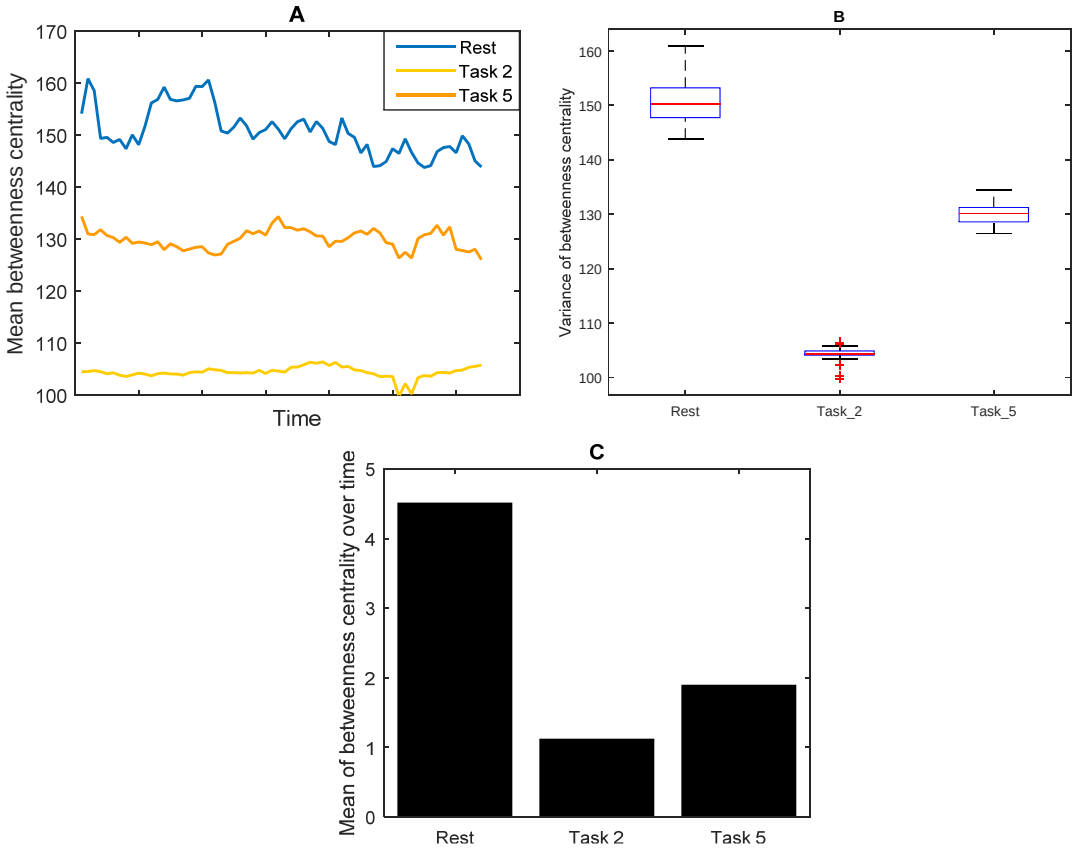

Figure 16 - Variability of mean betweenness centrality of Rest, Task 2 and Task 5 networks. (A) Mean betweenness centrality over time. (B) Result of the Bartlett's test for equality of variances. (C) Mean betweenness centrality variability measured as coefficient of variation of betweenness centrality over time.

3.4.3 | Functional integration and segregation

Results of global efficiency, a measure of functional integration, and local efficiency, an estimate of functional segregation, are presented in Figure 17 and Figure 18, respectively.

A one-way ANOVA revealed a significant effect of task on global efficiency mean ($F(2,189) = 479680.28$, $P < 0.001$); post hoc testing revealed the following significant differences: Task 2 > Task 5 > Rest. Using a Bartlett's test we did not find a significant effect of task on global efficiency variance.

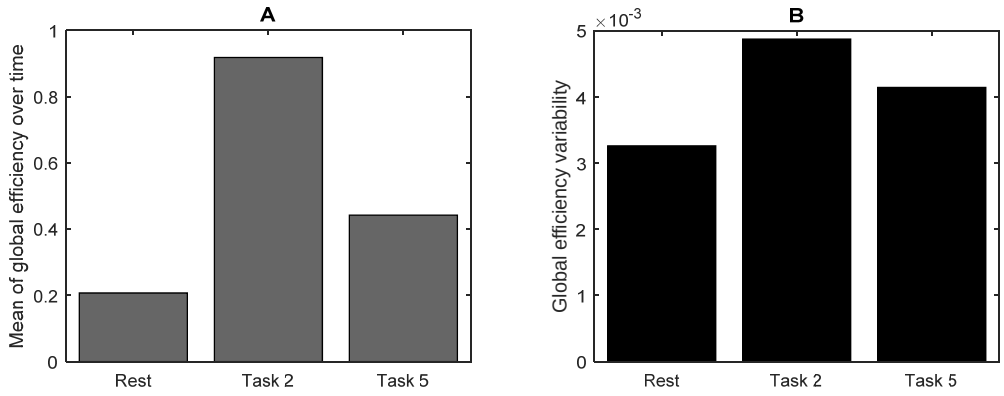

Figure 17 – Global efficiency (A) mean and (B) variability over time, in Rest, Task 2 and Task 5 networks.

Regarding the mean of local efficiency, a one-way ANOVA revealed a significant effect of task on local efficiency mean ($F(2,189) = 477975.1$, $P < 0.001$)); post hoc testing revealed the following significant differences: Task 2 > Task 5 > Rest. Moreover, using a Bartlett's test we also found a significant effect of task on local efficiency variance ($F(2,192) = 44.7271$, $P < 0.001$), with post hoc testing revealing the following significant differences: Task 5 > Rest; Task 5 > Task 2.

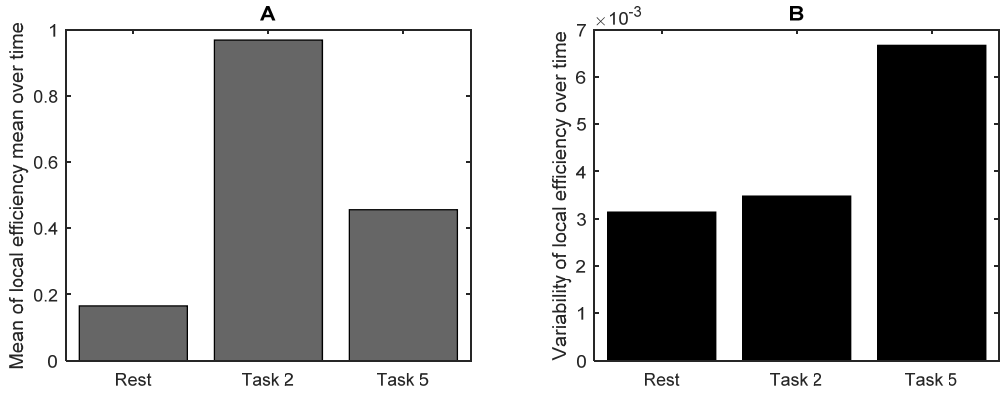

Figure 18 – Local efficiency (A) mean and (B) variability over time, in Rest, Task 2 and Task 5 networks.

Results obtained using sparsed binarized matrices of FC networks are displayed in Figure 19. There was a significant effect of brain state on global efficiency ($F(3,160) = 4.88$, $P < 0.001$). Post hoc testing indicated the following significant differences: Random > Rest > Task 5 > Task 2. On the contrary, there was not a significant effect on local efficiency.

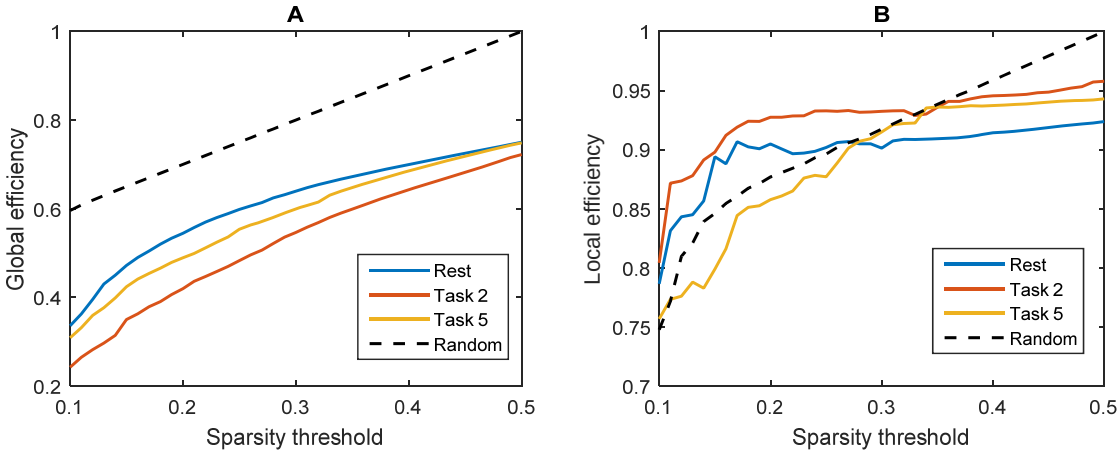

Figure 19 – Global (A) and local (B) efficiency for Rest, Task 2, Task 5 and random networks, as a function of connectivity sparsity.

4 | Discussion

In the present thesis, we used a computational model of resting-state brain activity to investigate the role of connectivity alterations in the global dynamics of the brain. Specifically, we inquired whether tuning of specific connections between brain regions might be able to trigger global dynamics changes that are observed during the performance of tasks. Two alterations of connectivity were performed and the resulting simulations' data were analysed to evaluate effects on FC mean and variability and graph measures. The results revealed that the task simulations were able to reproduce several aspects of the task global dynamics, although some features that characterize that state were not found.

4.1 | Computational model

The large-scale neural network model used was initially developed to explain the origin of spatiotemporal patterns of slow fluctuations observed in the BOLD signal during rest (Cabral et al. 2011). Although apparently too simplistic, this model has since been successful in simulating the global dynamics behaviour of the brain in several studies (Cabral et al. 2011, 2012, 2014, 2015, Hellyer et al. 2014). In general, results from these studies suggest that resting-state functional connectivity is largely shaped by structural coupling strength. Considering this, we altered specific structural connections to investigate whether such modifications would cause the model simulations to reproduce the global dynamics of a different brain mode: the task state.

4.2 | Simulation of task state: connectivity alterations

The first connectivity alteration was the augmentation of the strength of TPN efferent connections, to simulate the effect that the increase of these regions' activity, typically observed during tasks, has in the rest of the brain. This method, previously implemented by Hellyer et al. (2014), is based on the assumption that when a region is more active, it will increase communication with connected regions and therefore increase its efferent functional connectivity. Although this assumption is not straightforward, we decided to use this method since it had been successfully used by Hellyer et al. to simulate important global dynamics' changes associated with the cognitive states of task performance and rest.

The second connectivity alteration was the increase of strength of connections from DAN to VAN regions. This method is based on the assumption that signals from DAN to VAN suppress and filter out unimportant distracter information, which is supported by Wen et al. (2012) results, which revealed that increased Granger causality influences from DAN to VAN were correlated with enhanced task performance. Such findings are consistent with the hypothesis that anticipating the appearance and location of an object activates DAN (Kastner et al. 1999, Shulman et al. 1999, Corbetta et al. 2000, Hopfinger et al. 2000) and suppresses VAN (Shulman et al. 2003, Todd et al. 2005) and suggest, as the authors highlighted, a network-level mechanism of top-down control from DAN to VAN that suppresses VAN activity to filter out behaviourally irrelevant input and enhances the efficacy of sensori-motor processing. These considerations lead us to hypothesize that such a top-down control mechanism might contribute to trigger some of the task's changes in global dynamics.

4.3 | Functional connectivity analysis

After converting the simulated neural signals to BOLD signals, we were able to perform functional connectivity analysis and evaluate the effects of structural alterations.

To assess FC variability, we used not only standard deviation but also the coefficient of variation, which is useful since standard deviation must always be understood in the context of the data mean. The analysis revealed significant alterations for several of the simulated tasks, with some of these exhibiting a higher FC variability and others a lower variability. Since empirical evidence of FC variability measured as both standard deviation and

coefficient of variation has revealed a general decrease from rest to task states (Elton and Gao. 2015), we selected, from each set of simulated tasks originating from each method, the task that displayed a decrease in FC variability with both of the referred measures. The chosen tasks were Task 2 from the first method and Task 5 from the second method. Interestingly, for both of these tasks we used a multiplying factor of 4 when increasing connectivity strengths prior to simulations. The fact that different multiplying factors produce opposing effects – for instance, Tasks 1 and 4 (multiplying factor of 2) and 3 and 6 (multiplying factor of 8) produced a global increase in FC standard deviation, while Tasks 2 and 5 (multiplying factor of 4) generated a decrease in FC standard deviation – indicate that the tuning of connectivity strengths is critical to trigger the specific global dynamics' characteristics.

Granger causality analysis performed on the simulated tasks generated using the second method support the FC variability results, since only Task 5 presented a significant increase in influences from DAN to VAN.

Analysis of FC mean also revealed significant differences between rest and some of the simulated tasks. Notably, all tasks exhibiting such significant differences enhanced its FC mean relative to rest, with Task 2 and Task 5 revealing the most expressive increase. These results however are not in accordance with Elton and Gao's, which did not find any significant effects of task on FC mean.

4.4 | Graph theory analysis

To explore additional changes in the global behaviour of simulated task graphs, we evaluated several measures of graph theory in the two selected tasks (2 and 5).

Our results show an overall higher level of connection strength in the two task networks, comparing to rest, in accordance to Goparaju et al. (2014) findings. This result was expected since both tasks revealed increased FC mean. Moreover, the relationship in regional measures of strength and betweenness centrality between rest and task networks, evaluated by plotting each node strength in rest against the same node strength in task, revealed a radical change from one condition to the other. These results suggest a displacement of hubs (the most important nodes in a network) and a global change in the

topology of the networks. Goparaju et al. (2014) also reported a global hubs' shift, however this change was subtle rather than drastic.

The variability of these regional network measures was also assessed, revealing interesting results. Strength had a significant rise in standard deviation in both tasks, with Task 2 having a greater increase, however computation of the coefficient of variation revealed the opposing effect: a reduction in both tasks comparing to rest. Therefore, these results are difficult to interpret. Betweenness centrality however did not have this problem, since both standard deviation and coefficient of variation indicate a significant decrease in variability in the two tasks. This reduction indicates that comparing to rest, the topology of the brain in task state may be more stable over time, with fewer or less drastic hubs' displacements. This result is therefore in agreement with Elton and Gao (2015), which reported a significant decrease in the variability of several graph measures, suggesting a more stable topological dynamics over time.

Functional segregation and integration were evaluated using two methodologies: the first using weighted matrices and the second using threshold-binarized matrices. Results of weighted matrices reveal the same effect on the two tasks: both Task 2 and Task 5 increased segregation and integration by approximately the same factor, with Task 2 having a significantly greater augmentation than Task 5. These results do not agree with what is found in the literature: studies of rest vs. task graph theory analysis usually report either an increase in segregation and decrease in integration or an increase in segregation and decrease in integration. This results' discrepancy may be due to differences in methodology since the study of brain networks using graph theory is a very recent area and therefore multiple approaches have been experimented. In fact, binarized matrices originated in completely different results: the two tasks presented significantly decreased global efficiency and no change in local efficiency.

Variability analysis did not reveal differences in these measures, except for the segregation in Task 5, which was significantly increased, comparing to the other two simulations. From Elton and Gao (2015) findings, we expected measures of integration and segregation to decrease their variability.

Overall, graph theory results are not conclusive. Some of the measures reproduce empirical results, while others are opposing to what was expected from experimental studies. However, we must underline that many of these properties are distinctively evaluated in different studies, therefore, as previously stated, such discrepancy in results may be due to methodological differences.

4.5 | Limitations and future work

Since the results seem rather promising, further explorations should be made to test the hypotheses. Specifically, different methodologies should be experimented – for instance, functional connectivity variability should be tested using different window lengths – and more control simulations should be tested to ensure that the triggering effect of the increase of connectivity is regions-specific. Empirical studies should also be undertaken in order to explain the mechanisms by which functional connectivity strengths are increased.

We demonstrated the power of few structural alterations to generate a global significant change in the dynamics of the brain. However, we are aware that the connections considered are only a small part of the whole connectome that effectively undergoes functional connectivity changes. If more connections were considered, the parameters used, namely the multiplication factor by which connections were increased, would probably be different. Therefore, further investigations should increase the number of connectivity alterations, in order to more realistically represent the brain and its functional connectivity changes.

If successful, the ability to simulate *in silico* the attentional state of task is of high importance. Such simulations would provide a new tool for the study of alterations that negatively affect that state, with attention deficit hyperactivity disorder being an example, as well as possible improvement methods and techniques, such as meditation practice or pharmacological treatments.

5| Conclusion

In this thesis, we aimed to investigate mechanisms that may explain the observed alterations in the global dynamics of the brain in the focused attentional state of task. Inspired by empirical evidence, we hypothesized that changes in connectivity strength between and within attentional networks might be the trigger to the shift between the resting-state and the task state. Two possible mechanisms were evaluated using a computational model of the brain and produced promising results. The first is based on the idea that increased activity in one region will increase communication with the connected regions, thus augmenting efferent connections. Assuming this hypothesis, we increased efferent of connections of typically more active regions during tasks. The second mechanism explored was the increase of connectivity from DAN, a network associated with external attention focus, to VAN, a network that interrupts DAN's ongoing activity to direct attention to salient events. Hypothesizing that DAN might be able to suppress VAN's disturbing activity, we increased connectivity from the first network to the second. Notably, both mechanisms were able to produce global changes typically associated with the task state, including a reduced functional connectivity variability and an overall increased node strength. Simulations with similar connectivity alterations but involving different networks were performed to ensure that the differences observed were not due to random increase in connectivity, but rather to the specificity of the selected connections.

In conclusion, these findings suggest two mechanisms for switching between attentional states and raises hypotheses that can be tested in empirical studies. In particular, it would be interesting to determine if these mechanisms show inter-individual variability and are affected in individuals with attention deficits.

Appendix

A.I – Lists of regions in the AAL parcellation scheme

Table 1 – Abbreviations, names and MNI coordinates (in mm) of brain regions in the AAL parcellation scheme. L – left; R – right.

Brain region abbreviation	Brain region name	X	Y	Z
L Precentral	Precentral gyrus (motor, BA4)	-39,649571	-5,683325	50,944204
R Precentral		40,374566	-8,213061	52,092025
L Frontal Sup	Superior frontal gyrus	-19,445686	34,808127	42,201729
R Frontal Sup		20,899716	31,120103	43,815357
L Front Sup Orb	Superior frontal gyrus, orbital part	-17,560361	47,324667	-13,306768
R Front Sup Orb		17,494719	48,097977	-14,020104
L Front Mid	Middle frontal gyrus	-34,431796	32,731832	35,455581
R Front Mid		36,594838	33,061921	34,035097
L Front Mid Orb	Middle frontal gyrus, orbital pat	-31,645669	50,429696	-9,618954
R Front Mid Orb		32,181705	52,587936	-10,731165
L Front Inf Ope	Inferior frontal gyrus, pars opercularis	-49,433805	12,733285	19,022488
R Front Inf Ope		49,203956	14,976463	21,411759
L Front Inf Tri	Inferior frontal gyrus, pars triangularis	-46,583168	29,913997	13,9904
R Front Inf Tri		49,329734	30,161802	14,17336
L Front Inf Orb	Inferior frontal gyrus, pars orbitalis	-36,984842	30,707432	-12,109787
R Front Inf Orb		40,224413	32,230305	-11,910962
L Rolandic Oper	Rolandic operculum	-48,158458	-8,475501	13,950749
R Rolandic Oper		51,64679	-6,252213	14,634678
L Supp Motor Ar	Supplementary motor area	-6,324037	4,848455	61,375477
R Supp Motor Ar		7,61578	0,171406	61,853799
L Olfactory	Olfactory cortex	-9,062776	15,05305	-11,455349
R Olfactory		9,426947	15,912073	-11,256343
L Front Sup Med	Medial frontal gyrus	-5,79943	49,168665	30,893678
R Front Sup Med		8,099358	50,840627	30,21933
L Front Med Orb	Medial orbitofrontal cortex	-6,174033	54,057148	-7,396754
R Front Med Orb		7,161135	51,671033	-7,134061
L Rectus	Gyrus rectus	-6,081876	37,072407	-18,136218

R Rectus		7,353288	35,644688	-18,044013
L Insula	Insula	-36,130982	6,65178	3,440932
R Insula		38,019111	6,245116	2,077506
L Cingulum Ant	Anterior cingulate gyrus	-5,036584	35,399858	13,952874
R Cingulum Ant		7,45566	37,005554	15,839782
L Cingulum Mid	Midcingulate area	-6,476405	-14,919804	41,56943
R Cingulum Mid		7,020353	-8,826396	39,791022
L Cingulum Post	Posterior cingulate gyrus	-5,847645	-42,9179	24,669717
R Cingulum Post		6,437453	-41,814996	21,866616
L Hippocampus	Hippocampus	-26,026777	-20,741197	-10,133485
R Hippocampus		28,230739	-19,783197	-10,331186
L ParaHippocamp	Parahippocampal gyrus	-22,171081	-15,950323	-20,704347
R ParaHippocamp		24,381812	-15,146766	-20,470204
L Amygdala	Amygdala	-24,268898	-0,667051	-17,141373
R Amygdala		26,319084	0,638677	-17,502799
L Calcarine	Calcarine sulcus	-8,141653	-78,66696	6,439225
R Calcarine		14,994222	-73,148337	9,40477
L Cuneus	Cuneus	-6,933982	-80,133603	27,223523
R Cuneus		12,510995	-79,358209	28,228385
L Lingual	Lingual gyrus	-15,616938	-67,554985	-4,632884
R Lingual		15,289864	-66,925854	-3,874743
L Occipital Sup	Superior occipital gyrus	-17,540728	-84,262256	28,165323
R Occipital Sup		23,291506	-80,853888	30,586958
L Occipital Mid	Middle occipital gyrus	-33,388511	-80,731617	16,114779
R Occipital Mid		36,387657	-79,704639	19,415758
L Occipital Inf	Inferior occipital gyrus	-37,358678	-78,292994	-7,844347
R Occipital Inf		37,158658	-81,993063	-7,613192
L Fusiform	Fusiform gyrus	-32,159276	-40,297769	-20,228222
R Fusiform		32,968062	-39,101745	-20,178425
L Postcentral	Postcentral gyrus	-43,462371	-22,63134	48,917238
R Postcentral		40,428357	-25,493051	52,544956
L Parietal Sup	Superior parietal lobule	-24,453599	-59,557237	58,960107
R Parietal Sup		25,105845	-59,179845	62,061752
L Parietal Inf	Inferior parietal lobule	-43,803723	-45,819664	46,740526
R Parietal Inf		45,462046	-46,289696	49,535074
L SupraMarginal	Supramarginal gyrus	-56,78813	-33,637832	30,44948
R SupraMarginal		56,610717	-31,504883	34,479962
L Angular	Angular gyrus	-45,141308	-60,815849	35,587244
R Angular		44,507674	-59,984653	38,627668
L Precuneus	Precuneus	-8,240849	-56,070915	48,009027
R Precuneus		8,979604	-56,049496	43,769428
L Paracentr Lob	Paracentral lobule	-8,63015	-25,364585	70,070294
R Paracentr Lob		6,477066	-31,587031	68,094128
L Caudate	Caudate nucleus	-12,461859	10,995965	9,23913
R Caudate		13,836167	12,074298	9,415187
L Putamen	Putamen	-24,91375	3,855326	2,401284
R Putamen		26,778731	4,912926	2,464747
L Pallidum	Globus pallidus	-18,749672	-0,03151	0,210503
R Pallidum		20,20064	0,175503	0,228062
L Thalamus	Thalamus	-11,848391	-17,564483	7,976092
R Thalamus		11,997738	-17,552447	8,086796

L Heschl	Transverse temporal gyrus	-42,991685	-18,875277	9,978381
R Heschl		44,856921	-17,146694	10,405992
L Temporal Sup	Superior temporal gyrus	-54,156498	-20,677555	7,134812
R Temporal Sup		57,145974	-21,780584	6,80137
L Tempr Pol Sup	Superior temporal pole	-40,878569	15,144114	-20,182734
R Tempr Pol Sup		47,246762	14,745166	-16,863244
L Temporal Mid	Middle temporal gyrus	-56,523899	-33,799812	-2,200976
R Temporal Mid		56,473481	-37,22799	-1,46807
L Tempr Pol Mid	Middle temporal pole	-37,319853	14,586898	-34,080882
R Tempr Pol Mid		43,22038	14,551637	-32,233157
L Temporal Inf	Inferior temporal gyrus	-50,770655	-28,051624	-23,168441
R Temporal Inf		52,692181	-31,069236	-22,318884

Table 2 – Regions-of-interest defining each brain network. B – bilateral; R – right.

DAN	B Parietal sup
	B Occipital inf
	B Precentral
VAN	R Front mid
	R Front inf ope
	R Angular
DMN	B Cingulum post
	B Front sup med
	B Angular
Visual	B Calcarine
	B Cuneus
	B Occipital mid
Somatomotor	B Precentral
	B Supp motor ar
	B Postcentral

A.II – FC variability in control simulations

Figure 20 displays the results of FC variability analysis in simulated tasks resulting from the increase of strength of DMN efferent connections, while Figure 21 presents the results from tasks resulting from strength increase of connections from DAN to DMN. As can be visually perceived, results from these tasks are significatively different from those obtained from tasks 1-6.

Variability of sliding window FC

A

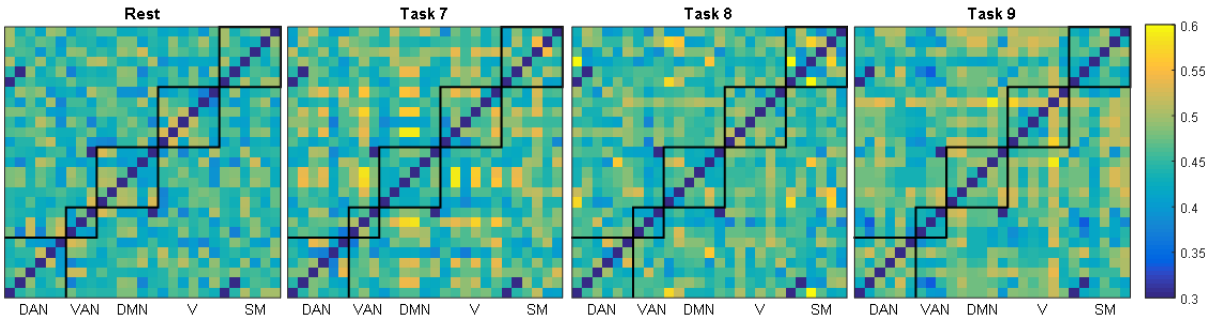

B

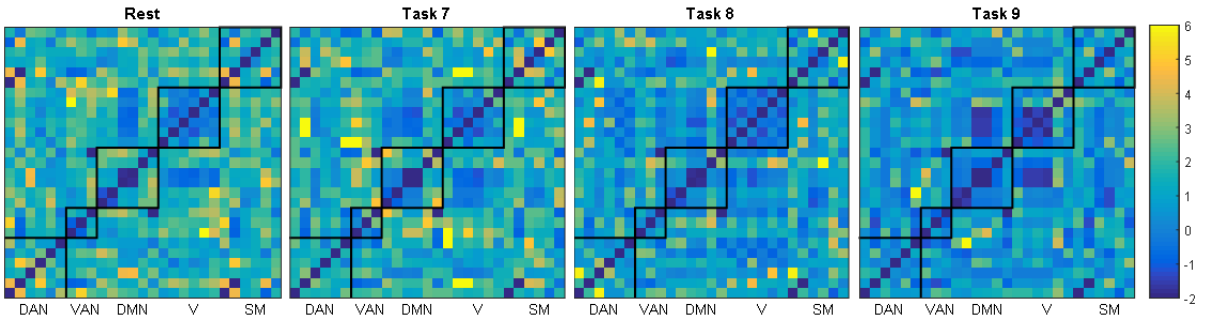

Figure 20 - Matrices of the effect of task on FC sliding window time series, including (A) standard deviation, (B) coefficient of variation and (C) mean. Within-network connectivities are underlined in black boxes.

Variability of sliding window FC

A

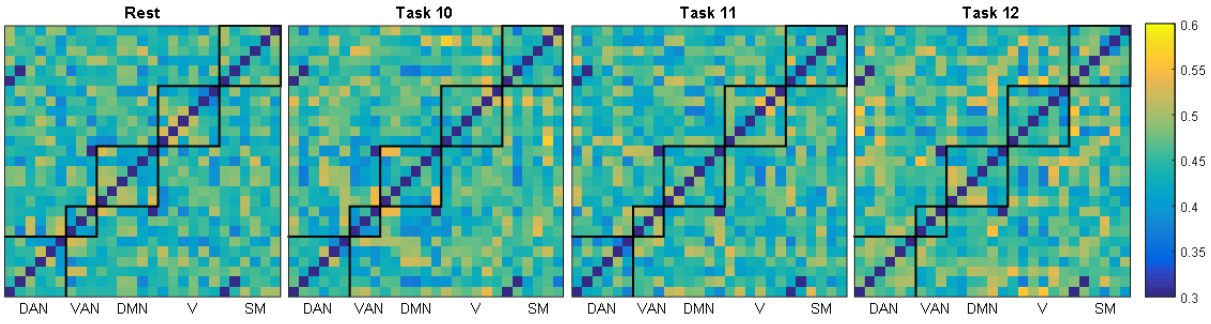

B

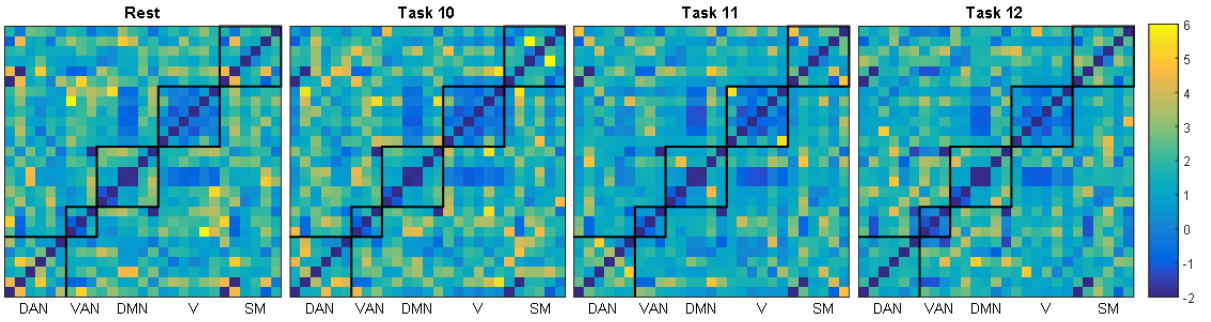

Figure 21 - Matrices of the effect of task on FC sliding window time series, including (A) standard deviation, (B) coefficient of variation and (C) mean. Within-network connectivities are underlined in black boxes.

References

Addis, D. R., Sacchetti, D. C., Ally, B. A., Budson, A. E., & Schacter, D. L. (2009). Episodic simulation of future events is impaired in mild Alzheimer's disease. *Neuropsychologia*, *47*(12), 2660-2671.

Addis, D. R., Wong, A. T., & Schacter, D. L. (2007). Remembering the past and imagining the future: Common and distinct neural substrates during event construction and elaboration. *Neuropsychologia*, *45*(7), 1363-1377.

Andreasen, N. C., O'Leary, D. S., Cizadlo, T., Arndt, S., Rezai, K., Watkins, G. L., ... & Hichwa, R. D. (1995). Remembering the past: two facets of episodic memory explored with positron emission tomography. *The American journal of psychiatry* 152: 1576-1585

Andrews-Hanna, J. R., Reidler, J. S., Sepulcre, J., Poulin, R., & Buckner, R. L. (2010). Functional-anatomic fractionation of the brain's default network.*Neuron*, *65*(4), 550-562.

Andrews-Hanna, J. R., Smallwood, J., & Spreng, R. N. (2014). The default network and self-generated thought: component processes, dynamic control, and clinical relevance. *Annals of the New York Academy of Sciences*,*1316*(1), 29-52.

Andrews-Hanna, J. R., Snyder, A. Z., Vincent, J. L., Lustig, C., Head, D., Raichle, M. E., & Buckner, R. L. (2007). Disruption of large-scale brain systems in advanced aging. *Neuron*, *56*(5), 924-935.

Anticevic, A., Brumbaugh, M. S., Winkler, A. M., Lombardo, L. E., Barrett, J., Corlett, P. R., ... & Glahn, D. C. (2013). Global prefrontal and fronto-amygdala dysconnectivity in bipolar I disorder with psychosis history. *Biological psychiatry*, *73*(6), 565-573.

Anticevic, A., Cole, M. W., Murray, J. D., Corlett, P. R., Wang, X. J., & Krystal, J. H. (2012). The role of default network deactivation in cognition and disease.*Trends in cognitive sciences*, *16*(12), 584-592.

Baird, B., Smallwood, J., Mrazek, M. D., Kam, J. W., Franklin, M. S., & Schooler, J. W. (2012). Inspired by distraction mind wandering facilitates creative incubation. *Psychological Science*, 0956797612446024.

Banich, M. T. (2009). Executive function the search for an integrated account. *Current Directions in Psychological Science*, *18*(2), 89-94.

Barnard, P. J., & Teasdale, J. D. (1991). Interacting cognitive subsystems: A systemic approach to cognitive-affective interaction and change. *Cognition & Emotion*, *5*(1), 1-39.

Barnett, L., & Seth, A. K. (2014). The MVGC multivariate Granger causality toolbox: a new approach to Granger-causal inference. *Journal of neuroscience methods*, *223*, 50-68.

Barron, E., Riby, L. M., Greer, J., & Smallwood, J. (2011). Absorbed in thought the effect of mind wandering on the processing of relevant and irrelevant events. *Psychological science*.

Binder, J. R., Frost, J. A., Hammeke, T. A., Bellgowan, P. S. F., Rao, S. M., & Cox, R. W. (1999). Conceptual processing during the conscious resting state: a functional MRI study. *Journal of cognitive neuroscience*, *11*(1), 80-93.

Botzung, A., Denkova, E., & Manning, L. (2008). Experiencing past and future personal events: Functional neuroimaging evidence on the neural bases of mental time travel. *Brain and cognition*, *66*(2), 202-212.

Buckner, R. L., & Carroll, D. C. (2007). Self-projection and the brain. *Trends in cognitive sciences*, *11*(2), 49-57.

Buckner, R. L., Andrews-Hanna, J. R., & Schacter, D. L. (2008). The brain's default network. *Annals of the New York Academy of Sciences*, *1124*(1), 1-38.

Buckner, R. L., Snyder, A. Z., Shannon, B. J., LaRossa, G., Sachs, R., Fotenos, A. F., ... & Mintun, M. A. (2005). Molecular, structural, and functional characterization of Alzheimer's disease: evidence for a relationship between default activity, amyloid, and memory. *The Journal of Neuroscience*, *25*(34), 7709-7717.

Buhle, J. T., Silvers, J. A., Wager, T. D., Lopez, R., Onyemekwu, C., Kober, H., ... & Ochsner, K. N. (2014). Cognitive reappraisal of emotion: a meta-analysis of human neuroimaging studies. *Cerebral Cortex*, *24*(11), 2981-2990.

Christoff, K., Gordon, A. M., Smallwood, J., Smith, R., & Schooler, J. W. (2009). Experience sampling during fMRI reveals default network and executive system contributions to mind wandering. *Proceedings of the National Academy of Sciences*, *106*(21), 8719-8724.

Cole, M. W., Reynolds, J. R., Power, J. D., Repovs, G., Anticevic, A., & Braver, T. S. (2013). Multi-task connectivity reveals flexible hubs for adaptive task control. *Nature neuroscience*, *16*(9), 1348-1355.

Corbetta, M., & Shulman, G. L. (2002). Control of goal-directed and stimulus-driven attention in the brain. *Nature reviews neuroscience*, *3*(3), 201-215.

Damoiseaux, J. S., Beckmann, C. F., Arigita, E. S., Barkhof, F., Scheltens, P., Stam, C. J., ... & Rombouts, S. A. R. B. (2008). Reduced resting-state brain activity in the “default network” in normal aging. *Cerebral cortex*, *18*(8), 1856-1864.

Daselaar, S. M., Prince, S. E., & Cabeza, R. (2004). When less means more: deactivations during encoding that predict subsequent memory.*Neuroimage*, *23*(3), 921-927.

Daselaar, S. M., Prince, S. E., Dennis, N. A., Hayes, S. M., Kim, H., & Cabeza, R. (2009). Posterior midline and ventral parietal activity is associated with retrieval success and encoding failure. *Frontiers in human neuroscience*, *3*.

Depue, B. E., Curran, T., & Banich, M. T. (2007). Prefrontal regions orchestrate suppression of emotional memories via a two-phase process.*science*, *317*(5835), 215-219.

Dosenbach, N. U., Visscher, K. M., Palmer, E. D., Miezin, F. M., Wenger, K. K., Kang, H. C., ... & Petersen, S. E. (2006). A core system for the implementation of task sets. *Neuron*, *50*(5), 799-812.

Eichele, T., Debener, S., Calhoun, V. D., Specht, K., Engel, A. K., Hugdahl, K., ... & Ullsperger, M. (2008). Prediction of human errors by maladaptive changes in event-related brain networks. *Proceedings of the National Academy of Sciences*, *105*(16), 6173-6178.

Etkin, A., Egner, T., & Kalisch, R. (2011). Emotional processing in anterior cingulate and medial prefrontal cortex. *Trends in cognitive sciences*, *15*(2), 85-93.

Fletcher, P. C., Happe, F., Frith, U., Baker, S. C., Dolan, R. J., Frackowiak, R. S., & Frith, C. D. (1995). Other minds in the brain: a functional imaging study of "theory of mind" in story comprehension. *Cognition*, *57*(2), 109-128.

Fox, M. D., Snyder, A. Z., Vincent, J. L., Corbetta, M., Van Essen, D. C., & Raichle, M. E. (2005). The human brain is intrinsically organized into dynamic, anticorrelated functional networks. *Proceedings of the National Academy of Sciences of the United States of America*, *102*(27), 9673-9678.

Freeman, L. C. (1978). Centrality in social networks conceptual clarification.*Social networks*, *1*(3), 215-239.

Gao, W., Gilmore, J. H., Shen, D., Smith, J. K., Zhu, H., & Lin, W. (2013). The synchronization within and interaction between the default and dorsal attention networks in early infancy. *Cerebral cortex*, *23*(3), 594-603.

Greene, J. D., Sommerville, R. B., Nystrom, L. E., Darley, J. M., & Cohen, J. D. (2001). An fMRI investigation of emotional engagement in moral judgment.*Science*, *293*(5537), 2105-2108.

Greene, J., & Haidt, J. (2002). How (and where) does moral judgment work?.*Trends in cognitive sciences*, *6*(12), 517-523.

Greicius, M. D., Flores, B. H., Menon, V., Glover, G. H., Solvason, H. B., Kenna, H., ... & Schatzberg, A. F. (2007). Resting-state functional connectivity in major depression: abnormally increased contributions from subgenual cingulate cortex and thalamus. *Biological psychiatry*, *62*(5), 429-437.

Greicius, M. D., Krasnow, B., Reiss, A. L., & Menon, V. (2003). Functional connectivity in the resting brain: a network analysis of the default mode hypothesis. *Proceedings of the National Academy of Sciences*, *100*(1), 253-258.

Gusnard, D. A., Akbudak, E., Shulman, G. L., & Raichle, M. E. (2001). Medial prefrontal cortex and self-referential mental activity: relation to a default mode of brain function. *Proceedings of the National Academy of Sciences*,*98*(7), 4259-4264.

Hagmann, P., Cammoun, L., Gigandet, X., Meuli, R., Honey, C. J., Wedeen, V. J., & Sporns, O. (2008). Mapping the structural core of human cerebral cortex. *PLoS Biol*, *6*(7), e159.

Hare, T. A., Camerer, C. F., & Rangel, A. (2009). Self-control in decision-making involves modulation of the vmPFC valuation system. *Science*,*324*(5927), 646-648.

Harrison, B. J., Soriano-Mas, C., Pujol, J., Ortiz, H., López-Solà, M., Hernández-Ribas, R., ... & Cardoner, N. (2009). Altered corticostriatal functional connectivity in obsessive-compulsive disorder. *Archives of general psychiatry*, *66*(11), 1189-1200.

Honey, C. J., Sporns, O., Cammoun, L., Gigandet, X., Thiran, J. P., Meuli, R., & Hagmann, P. (2009). Predicting human resting-state functional connectivity from structural connectivity. *Proceedings of the National Academy of Sciences*, *106*(6), 2035-2040.

Irish, M., Hornberger, M., Lah, S., Miller, L., Pengas, G., Nestor, P. J., ... & Piguet, O. (2011). Profiles of recent autobiographical memory retrieval in semantic dementia, behavioural-variant frontotemporal dementia, and Alzheimer's disease. *Neuropsychologia*, *49*(9), 2694-2702.

Jarrell, T. A., Wang, Y., Bloniarz, A. E., Brittin, C. A., Xu, M., Thomson, J. N., ... & Emmons, S. W. (2012). The connectome of a decision-making neural network. *Science*, *337*(6093), 437-444.

Kam, J. W., Dao, E., Farley, J., Fitzpatrick, K., Smallwood, J., Schooler, J. W., & Handy, T. C. (2011). Slow fluctuations in attentional control of sensory cortex. *Journal of cognitive neuroscience*, *23*(2), 460-470.

Kam, J. W., Xu, J., & Handy, T. C. (2014). I don't feel your pain (as much): the desensitizing effect of mind wandering on the perception of others' discomfort. *Cognitive, Affective, & Behavioral Neuroscience*, *14*(1), 286-296.

Kelly, A. C., Uddin, L. Q., Biswal, B. B., Castellanos, F. X., & Milham, M. P. (2008). Competition between functional brain networks mediates behavioral variability. *Neuroimage*, *39*(1), 527-537.

Koch, M. A., Norris, D. G., & Hund-Georgiadis, M. (2002). An investigation of functional and anatomical connectivity using magnetic resonance imaging.*Neuroimage*, *16*(1), 241-250.

Li, C. S. R., Yan, P., Bergquist, K. L., & Sinha, R. (2007). Greater activation of the "default" brain regions predicts stop signal errors. *Neuroimage*, *38*(3), 640-648.

Macdonald, J. S. P., Mathan, S., & Yeung, N. (2011). Frontiers: Trial-by-Trial Variations in Subjective Attentional State are Reflected in Ongoing Prestimulus EEG Alpha Oscillations. *Frontiers in Perception Science*, *2*.

Mason, M. F., Norton, M. I., Van Horn, J. D., Wegner, D. M., Grafton, S. T., & Macrae, C. N. (2007). Wandering minds: the default network and stimulus-independent thought. *Science*, *315*(5810), 393-395.

Mazoyer, B., Zago, L., Mellet, E., Bricogne, S., Etard, O., Houde, O., ... & Tzourio-Mazoyer, N. (2001). Cortical networks for working memory and executive functions sustain the conscious resting state in man. *Brain research bulletin*, *54*(3), 287-298.

Mckiernan, K. A., Kaufman, J. N., Kucera-Thompson, J., & Binder, J. R. (2003). A parametric manipulation of factors affecting task-induced deactivation in functional neuroimaging. *Journal of cognitive neuroscience*,*15*(3), 394-408.

Mega, M. S., Cummings, J. L., Fiorello, T., & Gornbein, J. (1996). The spectrum of behavioral changes in Alzheimer's disease. *Neurology*, *46*(1), 130-135.

Moreau, N., Viallet, F., & Champagne-Lavau, M. (2013). Using memories to understand others: The role of episodic memory in theory of mind impairment in Alzheimer disease. *Ageing research reviews*, *12*(4), 833-839.

Napadow, V., LaCount, L., Park, K., As-Sanie, S., Clauw, D. J., & Harris, R. E. (2010). Intrinsic brain connectivity in fibromyalgia is associated with chronic pain intensity. *Arthritis & Rheumatism*, *62*(8), 2545-2555.

Niendam, T. A., Laird, A. R., Ray, K. L., Dean, Y. M., Glahn, D. C., & Carter, C. S. (2012). Meta-analytic evidence for a superordinate cognitive control network subserving diverse executive functions. *Cognitive, Affective, & Behavioral Neuroscience*, *12*(2), 241-268.

Ochsner, K. N., Silvers, J. A., & Buhle, J. T. (2012). Functional imaging studies of emotion regulation: a synthetic review and evolving model of the cognitive control of emotion. *Annals of the New York Academy of Sciences*,*1251*(1), E1-E24.

Ogawa, Seiji, et al. "Brain magnetic resonance imaging with contrast dependent on blood oxygenation." *Proceedings of the National Academy of Sciences* 87.24 (1990): 9868-9872.

Okuda, J., Fujii, T., Ohtake, H., Tsukiura, T., Tanji, K., Suzuki, K., ... & Yamadori, A. (2003). Thinking of the future and past: The roles of the frontal pole and the medial temporal lobes. *Neuroimage*, *19*(4), 1369-1380.

Otten, L. J., & Rugg, M. D. (2001). When more means less: neural activity related to unsuccessful memory encoding. *Current Biology*, *11*(19), 1528-1530.

Partiot, A., Grafman, J., Sadato, N., Wachs, J., & Hallett, M. (1995). Brain activation during the generation of nonemotional and emotional plans.*Neuroreport*, *6*(10), 1397-1400.

Peters, J., & Büchel, C. (2010). Episodic future thinking reduces reward delay discounting through an enhancement of prefrontal-mediotemporal interactions. *Neuron*, *66*(1), 138-148.

Power, J. D., Cohen, A. L., Nelson, S. M., Wig, G. S., Barnes, K. A., Church, J. A., ... & Petersen, S. E. (2011). Functional network organization of the human brain. *Neuron*, *72*(4), 665-678.

Prebble, S. C., Addis, D. R., & Tippett, L. J. (2013). Autobiographical memory and sense of self. *Psychological bulletin*, *139*(4), 815.

Raichle, M. E., MacLeod, A. M., Snyder, A. Z., Powers, W. J., Gusnard, D. A., & Shulman, G. L. (2001). A default mode of brain function. *Proceedings of the National Academy of Sciences*, *98*(2), 676-682.

Rilling, J. K., Sanfey, A. G., Aronson, J. A., Nystrom, L. E., & Cohen, J. D. (2004). The neural correlates of theory of mind within interpersonal interactions. *Neuroimage*, *22*(4), 1694-1703.

Rubinov, M., & Sporns, O. (2010). Complex network measures of brain connectivity: uses and interpretations. *Neuroimage*, *52*(3), 1059-1069.

Sambataro, F., Wolf, N. D., Pennuto, M., Vasic, N., & Wolf, R. C. (2014). Revisiting default mode network function in major depression: evidence for disrupted subsystem connectivity. *Psychological medicine*, *44*(10), 2041-2051.

Saxe, R., & Kanwisher, N. (2003). People thinking about thinking people: the role of the temporo-parietal junction in "theory of mind". *Neuroimage*, *19*(4), 1835-1842.

Saxe, R., Carey, S., & Kanwisher, N. (2004). Understanding other minds: linking developmental psychology and functional neuroimaging. *Annu. Rev. Psychol.*, *55*, 87-124.

Schacter, D. L., Addis, D. R., & Buckner, R. L. (2007). Remembering the past to imagine the future: the prospective brain. *Nature Reviews Neuroscience*,*8*(9), 657-661.

Shannon, B. J., Dosenbach, R. A., Su, Y., Vlassenko, A. G., Larson-Prior, L. J., Nolan, T. S., ... & Raichle, M. E. (2013). Morning-evening variation in human brain metabolism and memory circuits. *Journal of neurophysiology*,*109*(5), 1444-1456.

Sheline, Y. I., Barch, D. M., Price, J. L., Rundle, M. M., Vaishnavi, S. N., Snyder, A. Z., ... & Raichle, M. E. (2009). The default mode network and self-referential processes in depression. *Proceedings of the National Academy of Sciences*, *106*(6), 1942-1947.

Sheline, Y. I., Price, J. L., Yan, Z., & Mintun, M. A. (2010). Resting-state functional MRI in depression unmasks increased connectivity between networks via the dorsal nexus. *Proceedings of the National Academy of Sciences*, *107*(24), 11020-11025.

Shulman, G. L., Fiez, J. A., Corbetta, M., Buckner, R. L., Miezin, F. M., Raichle, M. E., & Petersen, S. E. (1997). Common blood flow changes across visual tasks: II. Decreases in cerebral cortex. *Journal of cognitive neuroscience*,*9*(5), 648-663.

Simpson, J. R., Drevets, W. C., Snyder, A. Z., Gusnard, D. A., & Raichle, M. E. (2001). Emotion-induced changes in human medial prefrontal cortex: II. During anticipatory anxiety. *Proceedings of the National Academy of Sciences*, *98*(2), 688-693.

Singh, K. D., & Fawcett, I. P. (2008). Transient and linearly graded deactivation of the human default-mode network by a visual detection task.*Neuroimage*, *41*(1), 100-112.

Smallwood, J., & Andrews-Hanna, J. (2013). Not all minds that wander are lost: the importance of a balanced perspective on the mind-wandering state.*Frontiers in psychology*, *4*.

Smallwood, J., Beach, E., Schooler, J. W., & Handy, T. C. (2008). Going AWOL in the brain: Mind wandering reduces cortical analysis of external events. *Journal of cognitive neuroscience*, *20*(3), 458-469.

Smith, S. M. (2012). The future of FMRI connectivity. *Neuroimage*, *62*(2), 1257-1266.

Smith, S. M., Miller, K. L., Salimi-Khorshidi, G., Webster, M., Beckmann, C. F., Nichols, T. E., ... & Woolrich, M. W. (2011). Network modelling methods for FMRI. *Neuroimage*, *54*(2), 875-891.

Sporns, O., Tononi, G., & Edelman, G. M. (2000). Connectivity and complexity: the relationship between neuroanatomy and brain dynamics.*Neural Networks*, *13*(8), 909-922.

Spreng, R. N., & Schacter, D. L. (2012). Default network modulation and large-scale network interactivity in healthy young and old adults. *Cerebral Cortex*, *22*(11), 2610-2621.

Spreng, R. N., & Turner, G. R. (2013). Structural covariance of the default network in healthy and pathological aging. *The Journal of Neuroscience*,*33*(38), 15226-15234.

Spreng, R. N., Sepulcre, J., Turner, G. R., Stevens, W. D., & Schacter, D. L. (2013). Intrinsic architecture underlying the relations among the default, dorsal attention, and frontoparietal control networks of the human brain.*Journal of cognitive neuroscience*, *25*(1), 74-86.

Spreng, R. N., Stevens, W. D., Chamberlain, J. P., Gilmore, A. W., & Schacter, D. L. (2010). Default network activity, coupled with the frontoparietal control network, supports goal-directed cognition. *Neuroimage*, *53*(1), 303-317.

Stern, E. R., Fitzgerald, K. D., Welsh, R. C., Abelson, J. L., & Taylor, S. F. (2012). Resting-state functional connectivity between fronto-parietal and default mode networks in obsessive-compulsive disorder. *PloS one*, *7*(5), e36356.

Svoboda, E., McKinnon, M. C., & Levine, B. (2006). The functional neuroanatomy of autobiographical memory: a meta-analysis.*Neuropsychologia*, *44*(12), 2189-2208.

Sylvester, C. M., et al. "Functional network dysfunction in anxiety and anxiety disorders." *Trends in neurosciences* 35.9 (2012): 527-535.

Szpunar, K. K., Watson, J. M., & McDermott, K. B. (2007). Neural substrates of envisioning the future. *Proceedings of the National Academy of Sciences*,*104*(2), 642-647.

Toro, R., Fox, P. T., & Paus, T. (2008). Functional coactivation map of the human brain. *Cerebral cortex*, *18*(11), 2553-2559.

Varshney, L. R., Chen, B. L., Paniagua, E., Hall, D. H., & Chklovskii, D. B. (2011). Structural properties of the Caenorhabditis elegans neuronal network. *PLoS Comput Biol*, *7*(2), e1001066.

Vincent, J. L., Kahn, I., Snyder, A. Z., Raichle, M. E., & Buckner, R. L. (2008). Evidence for a frontoparietal control system revealed by intrinsic functional connectivity. *Journal of neurophysiology*, *100*(6), 3328-3342.

Vincent, J. L., Snyder, A. Z., Fox, M. D., Shannon, B. J., Andrews, J. R., Raichle, M. E., & Buckner, R. L. (2006). Coherent spontaneous activity identifies a hippocampal-parietal memory network. *Journal of neurophysiology*, *96*(6), 3517-3531.

Weissman, D. H., Roberts, K. C., Visscher, K. M., & Woldorff, M. G. (2006). The neural bases of momentary lapses in attention. *Nature neuroscience*,*9*(7), 971-978.

White, J. G., Southgate, E., Thomson, J. N., & Brenner, S. (1986). The structure of the nervous system of the nematode Caenorhabditis elegans: the mind of a worm. *Phil. Trans. R. Soc. Lond*, *314*, 1-340.

Whitfield-Gabrieli, S., & Ford, J. M. (2012). Default mode network activity and connectivity in psychopathology. *Annual review of clinical psychology*, *8*, 49-76.

Yeo, B. T., Krienen, F. M., Sepulcre, J., Sabuncu, M. R., Lashkari, D., Hollinshead, M., ... & Buckner, R. L. (2011). The organization of the human cerebral cortex estimated by intrinsic functional connectivity. *Journal of neurophysiology*, *106*(3), 1125-1165.